

Hallucinogen persisting perception disorder in neuronal networks with adaptation

Zachary P. Kilpatrick · G. Bard Ermentrout

Received: 19 January 2011 / Revised: 11 April 2011 / Accepted: 19 April 2011 / Published online: 14 June 2011
© Springer Science+Business Media, LLC 2011

Abstract We study the spatiotemporal dynamics of neuronal networks with spike frequency adaptation. In particular, we compare the effects of adaptation being either a linear or nonlinear function of neural activity. We find that altering parameters controlling the strength of synaptic connections in the network can lead to spatially structured activity suggestive of symptoms of hallucinogen persisting perception disorder (HPPD). First, we study how both networks track spatially homogeneous flickering stimuli, and find input is encoded as continuous at lower flicker frequencies when the network's synapses exhibit more net excitation. Mainly, we study instabilities of stimulus-driven traveling pulse solutions, representative of visual trailing phenomena common to HPPD patients. Visual trails are reported as discrete afterimages in the wake of a moving input. Thus, we analyze several solutions arising in response to moving inputs in both networks: an ON state, stimulus-locked pulses, and traveling breathers. We find traveling breathers can arise in both networks when an input moves beyond a critical speed. These possible neural substrates of visual trails occur at slower speeds when the modulation of synaptic connectivity is increased.

Keywords Hallucinations · Neuronal networks · Spike frequency adaptation · Traveling waves · Breathers

1 Introduction

Hallucinogen persisting perception disorder (HPPD) is a malfunction wherein past users of lysergic acid diethylamide (LSD) continue to see images reminiscent of drug induced hallucinations (Halpern and Pope 2003). Similar conditions have been described as the result of other hallucinogens like psilocybin, mescaline, and cannabis. Disturbances to visual experience persist long after the last ingestion of the hallucinogenic substance, up to weeks, months, and years. There is no strong correlation between the number of times a person has taken the drug and the likelihood that they develop HPPD, so the condition may result following a single LSD experience or never appear despite hundreds of LSD experiences (Abraham 1983). While the disorder was characterized close to thirty years ago, there are still open questions regarding its neural substrate and most appropriate treatment.

Abnormal brain states have long been known to result from the ingestion of LSD ever since Hoffman first synthesized the compound in 1938. In the decades that followed, a number of psychological experiments were carried out where subjects under the influence of LSD were studied as a drug-induced model of psychosis. Beginning in the 1960s, several studies of LSD users concluded that the hallucinogen could have long term effects on the brain like permanent visual disturbances, pre-schizophrenia, and thought disorder (Cohen and Ditman 1963; Rosenthal 1964; Frosch et al. 1965). As understanding of visual pathologies began to develop, Horowitz conducted a systematic study classifying three types of visual flashbacks: (i) *perceptual distortions* (e.g. seeing halos around objects); (ii) *heightened imagery* (visual experience is much more vivid and dominant

Action Editor: P. Dayan

Z. P. Kilpatrick (✉) · G. Bard Ermentrout
Department of Mathematics, University of Pittsburgh,
Pittsburgh, PA 15260, USA
e-mail: zpkilpat@pitt.edu

in one's thoughts); and (iii) *recurrent unbidden images* (subjects see objects that are not there) (Horowitz 1969).

Since these seminal studies, Abraham has characterized a wide range of visual pathologies arising from LSD usage. In particular, his systematic study of 123 previous LSD users in 1983 revealed much more detail regarding patterns in experience of patients suffering from HPPD. Some of the most common visual disturbances people report are spontaneous geometric hallucinations, intensification of color, trailing phenomena, halos around objects, and afterimages (Abraham 1983). The spontaneous geometric hallucinations include sparkles, lattices, and other complex patterns that are unsurprisingly similar to those seen during an actual LSD experience (Oster 1970). Trailing phenomena are positive afterimages left in the wake of an object as it moves across a subject's visual field. Abraham and Wolf extended these results to probe the effects of LSD on other aspects of visual function (Abraham and Wolf 1988). They found the critical frequency above which HPPD patients perceive flickering lights as being continuously on is lower than the average person's. In addition, adaptation to the dark takes significantly longer for a subject suffering from HPPD. The combination of these symptoms seems to suggest that HPPD arises due to alterations in synaptic connectivity involved in visual processing (Abraham and Duffy 1996).

Experimentalists continue to have difficulty pinpointing the precise neural seat of HPPD. It is important to note that HPPD subjects rarely ever believe visual experiences that they hallucinate are actually occurring (Abraham 1983). This suggests that the circuitry responsible for the disorder is not a higher brain area, but a lower visual area such as primary visual cortex (V1), the first cortical area responsible for geometric processing of visual input (Hubel and Wiesel 1977). Several theoretical studies of geometric visual hallucinations have built a remarkable case, based on the functional architecture of V1 and the retinocortical map, that such images are in fact generated in V1 (Ermentrout and Cowan 1979; Bressloff et al. 2001; Chossat and Faugeras 2009). Abraham and Duffy conducted an analysis comparing EEG spectra of awake subjects with and without HPPD, finding greater EEG coherence in visual regions for those with HPPD (Abraham and Duffy 2001). Nichols and Sanders-Bush found several genes are differentially expressed upon application of LSD to neural tissue (Nichols and Sanders-Bush 2002). They speculate that this combination of changes may be responsible for alteration in synaptic plasticity mechanisms, glutamatergic receptor expression, and cytoskeletal architecture. Together

these factors may contribute to a modulation of excitatory and inhibitory connections in visual areas.

A number of other phenomena induced by pharmaceuticals, brain damage, or neurological disorders bear resemblance to the visual disturbances of HPPD (Dubois and VanRullen 2011). For example, some patients taking antidepressants like nefazodone (Kraus 1996) and mirtazapine (Ihde-Scholl and Jefferson 2001) have reported palinopsia, where they see images after an actual visual stimulus has been removed. Interestingly, these and other antidepressants are known to increase extracellular levels of serotonin (Boyer and Shannon 2005), lending credence to the idea that similar visual disturbances due to LSD may arise from modulation of serotonin. Antiepileptic drugs like topiramate can also lead to visual trails described similarly to those seen in HPPD (Fontenelle 2008). Finally, Alzheimer's patients have been recently reported the experience of akinetopsia, where moving objects are perceived as a series of stills (Tsai and Mendez 2009). Thus, a firm understanding of visual disturbances due to HPPD would be valuable since the disorder is tied to a greater framework of visual pathologies whose neural substrates still remain ambiguous.

Based on quantitative psychological studies of HPPD, a number of pharmacological treatments have been administered to patients. Subjects taking benzodiazepines in particular experience an overall reduction in the intensity and frequency of visual disturbances (Abraham 1983). Lerner and colleagues used the benzodiazepine clonazepam, which is known to have serotonergic properties, so it may upregulate inhibition using serotonin receptors on inhibitory neurons (Lerner et al. 2001). Other successful pharmaceutical treatments include haloperidol, an extremely potent antipsychotic drug (Moskowitz 1971); sertraline, a known selective serotonin reuptake inhibitor (Young 1997); and clonidine, which acts on adrenergic receptors (Lerner et al. 1998). Conversely, phenothiazines, compounds known to block effects of dopamine, worsen conditions of HPPD (Abraham 1983). Thus, it appears there are many pathways to reducing the symptoms of HPPD, so the disorder may arise from either excess excitation or inhibition in visual networks.

In this paper we will examine the relative role alterations to synaptic neurotransmitter levels in the visual system can play in a theoretical model of trailing phenomena and halos linked to HPPD. Specifically, we will consider a paradigm where a light spot rotating in a circle is presented as visual input to a cortical network. We picture such a stimulus along with an HPPD subject's potential perception of the stimulus qualitatively based on previous research in Fig. 1(a). Were the

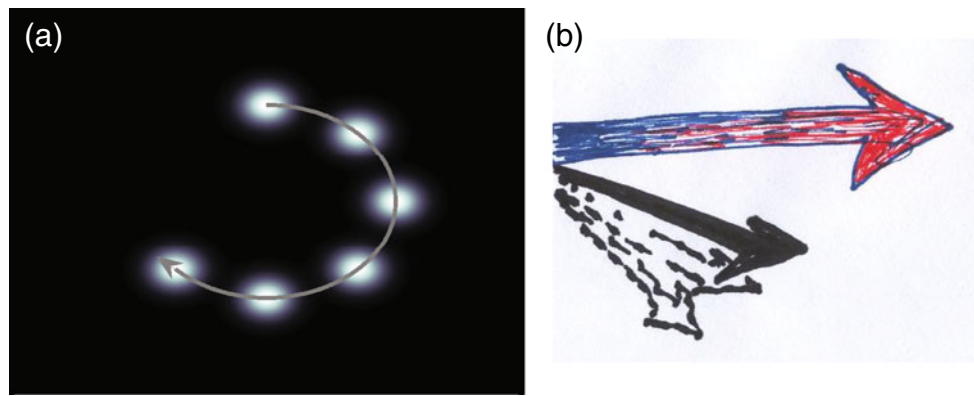


Fig. 1 (a) Snapshots of a spot of light rotating continuously on a circle. During visual trailing phenomena, one would see this not simply as a smoothly rotating light, but most likely discrete afterimages in addition to the smoothly rotating light image. They may also see a smudging out of the image, much like the tail of a comet. Halo phenomena lead to the observer seeing the light spot

as larger than it actually is. (b) Drawing of a single snapshot of visual experience by an HPPD patient watching an arrow rotating counterclockwise. The *blue and red arrow* is the representation of the arrow's actual location, and the *faint dark arrows* are the afterimages of the arrow left in its wake. Redrawn from H. D. Abraham (2011, personal communication)

network accurately resolving the stimulus, only neurons containing the light spot in their receptive field would represent it in visual cortex at any given point in time. Due to alterations in the neurotransmitter levels of visual cortex due to LSD usage, we presume neurons will represent the stimulus in regions addition to the area of presentation in an HPPD patient. Trails are represented by spatially discrete patches of neurons in the wake of the stimulus that fire for a period of time after input has been removed. A patient's own rendering of the discrete afterimages characteristic of visual trails are pictured in Fig. 1(b), when the stimulus is an arrow rotating counterclockwise (H. D. Abraham, 2011, personal communication). Halos may also appear around the object represented by neurons around the input being continuously on. All are potential realizations of HPPD in this simple stimulus paradigm.

Large-scale spatially structured activity such as the rotating spot of activity suggested by the above experimental setup is often modeled as a standing or traveling pulse of activity in neural field models of cortex (Wilson and Cowan 1972; Amari 1977). In these models, the evolution of mean firing rate in continuous space and time can be represented by a system of dynamical equations (Coombes 2005). These often appear as integrodifferential equations that incorporate specifics of the neural system in question with a particular synaptic connectivity (or weight) function, form of firing rate function, spatial domain, and auxiliary variables representing modifications to the mean population activity. Such systems can be analyzed extensively to determine how model functions and parameters relate to the existence of different solutions like traveling waves

(Pinto and Ermentrout 2001; Coombes and Owen 2004; Folias and Bressloff 2005b; Troy and Shusterman 2007), standing bumps (Amari 1977; Folias and Bressloff 2004; Guo et al. 2005), and patterns (Ermentrout and Cowan 1979; Bressloff et al. 2001; Laing and Troy 2003).

In particular, studies of traveling pulse dynamics often employ an auxiliary variable representing a negative feedback alternative other than synaptic inhibition (Pinto and Ermentrout 2001) because experiments that show disinhibited *in vitro* cortical slices support traveling pulses and spiral waves (Chervin et al. 1695; Huang et al. 2004). A common candidate for this negative feedback is spike frequency adaptation, resulting from calcium-dependent hyperpolarizing currents (Stocker et al. 1999; Benda and Herz 2003). There are justifiable ways to implement its dynamic effects as an additional subtractive variable in the activity equation of a neural field (Pinto and Ermentrout 2001; Coombes 2005; Kilpatrick and Bressloff 2010b). In neural field model studies, the auxiliary variable representing adaptation relates to the neural activity variable in either a *linear* or *nonlinear* manner. Pinto and Ermentrout introduced and analyzed the *linear* adaptation case on an infinite domain and found that for strong enough adaptation, traveling pulses exist in a neural field with purely excitatory synapses (Pinto and Ermentrout 2001). Since then, others have examined alternative solutions in the model like stimulus-induced breathers (Folias and Bressloff 2004, 2005b), spiral waves (Huang et al. 2004), multipulse solutions (Troy and Shusterman 2007), and self-sustained oscillations (Shusterman and Troy 2008). On the other hand, starting from three different conductance based models with an adaptation

current, Benda and Herz derived a neural field model where the relationship between neural activity and adaptation was *nonlinear* (Benda and Herz 2003). Hansel and Sompolinsky performed a mostly numerical study of the generation of traveling pulses of activity in networks in a periodic domain (a “ring” model) with nonlinear adaptation and stationary input (Hansel and Sompolinsky 1998). Coombes and Owen have analyzed spatially structured solutions of such a system in an infinite domain to find breathers, traveling pulses, and exotic solutions are generated through the inclusion of *nonlinear* adaptation (Coombes and Owen 2005). In Kilpatrick and Bressloff (2010b), it was shown that self-sustained oscillations also arise in a similar model. Thus, neural field models with adaptation have been utilized in describing a wide range of dynamics related to experimentally observed population level activity.

In this paper, we depart from previous studies by examining the dynamics resulting in a ring model with adaptation subject to rotating and stationary inputs. This is motivated by visual phenomena reported by patients suffering from HPPD, whose disorder we presume arises as the result of an alteration in the synaptic connectivity of visual cortex (Abraham 1983). In particular, we employ two different models, one with linear adaptation and the other with nonlinear adaptation as a means of comparison. The paper is organized as follows. We introduce both the model with linear adaptation and that with nonlinear adaptation in Section 2, pointing out their different functional forms. Then in Section 3, we carry out a detailed analysis of the stimulus-induced states resulting in the model with linear adaptation. Starting with a space-clamped version of the model we can develop conditions for when the whole network is always on in the limit of infinitely fast moving input as well as conditions for when the network is always on in the case of a spatially homogeneous input flickering on and off. We follow this with analyses of the spatially structured solutions of the network: the strictly on state, stimulus-locked traveling pulses, and stationary bumps. We find solutions representative of visual trails arise as traveling breathers, propagating pulse-like structures whose width oscillates. Halo-type solutions arise as activity profiles considerably wider than the stimulus input. Then, in Section 4, we present results of analysis of the network with nonlinear adaptation. A major difference with the case of linear adaptation is the stability analysis of traveling pulses in the network with nonlinear adaptation, whose details are presented in appendix. When the firing rate function is a Heaviside, ambiguous terms appear in the eigenmodes of the spectral calculation, which we resolve by noting that the terms will depend

on the sign of the perturbation applied to the traveling pulse. Finally, in Section 5, we show various numerical simulations of the both spatially extended networks along with extensions of analytic results to sigmoid and piecewise linear firing rate functions, different weight kernels, and different sized domains for comparison with our analysis.

2 Neuronal networks with adaptation

We consider two neuronal network models which each include spike frequency adaptation (Benda and Herz 2003; Madison and Nicoll 1984; Stocker et al. 1999). These are both set on a one-dimensional periodic domain according to the heuristic argument presented in the introduction regarding a possible diagnostic experiment of HPPD (see Fig. 1). First, we consider a model with negative feedback in the form of linear adaptation (Pinto and Ermentrout 2001):

$$\tau \frac{\partial u(x, t)}{\partial t} = -u(x, t) - v(x, t) + w * f(u) + I(x - ct), \quad (2.1a)$$

$$\alpha \frac{\partial v(x, t)}{\partial t} = -v(x, t) + \beta u(x, t), \quad (2.1b)$$

where

$$F * G = \int_{-\pi}^{\pi} F(x - x')G(x')dx'.$$

Equation (2.1a) describes the evolution of the synaptic current $u(x, t)$, with membrane time constant τ , in the presence of spike frequency adaptation, which takes the form of a subtractive linear term $v(x, t)$ evolving according to Eq. (2.1b). The spatial domain $x \in (-\pi, \pi)$ is periodic, which restricts the set of possible solutions u and v to have periodic boundary conditions. We consider larger periodic domains for x in the numerical solutions we perform in Section 5, finding most results do extend to a reasonable range of domain sizes. The functions f and w are the output firing rate (gain) function and strength of connections between neurons a distance $|x - x'|$ apart, respectively. We will define f , w , and I explicitly after we introduce the model with nonlinear adaptation, as they arise in this system as well. To specify visual input influenced by the rotating spot stimulus, we include the term $I(x - ct)$, which is invariant with respect to the wave coordinate $x - ct$ with propagation speed c . The adaptation current $v(x, t)$ is activated with strength β and time constant α (experimentally shown to be 40–120 ms (Madison and Nicoll 1984; Stocker et al. 1999)). Neural field models with linear spike frequency adaptation favor traveling

waves, especially in networks with no lateral inhibition (Hansel and Sompolinsky 1998; Pinto and Ermentrout 2001; Folias and Bressloff 2005b; Troy and Shusterman 2007; Kilpatrick et al. 2008).

In addition to the network with linear adaptation (2.1), we pursue study of a neuronal network with nonlinear adaptation. This type of model is especially motivated by the form of the adaptation current appearing in reduced firing rate models derived from more detailed conductance based models with outward hyperpolarizing currents (Benda and Herz 2003; Coombes and Owen 2005; Kilpatrick and Bressloff 2010b)

$$\tau \frac{\partial u(x, t)}{\partial t} = -u(x, t) + w * f(u - v) + I(x - ct), \quad (2.2a)$$

$$\alpha \frac{\partial v(x, t)}{\partial t} = -v(x, t) + \beta f(u(x, t) - v(x, t)). \quad (2.2b)$$

Equation (2.2a) describes the evolution of the synaptic current $u(x, t)$, with membrane time constant τ , in the presence spike frequency adaptation taking the form of an outward hyperpolarizing adaptation current $v(x, t)$ evolving according to Eq. (2.2b). Both u and v evolve on the periodic spatial domain $x \in (-\pi, \pi)$, but we also shall consider larger domains in Section 5. The adaptation current v is activated with strength β and time constant α (40–120 ms (Madison and Nicoll 1984; Stocker et al. 1999)). As derived from a universal adaptation current by Benda and Herz (2003), spike frequency adaptation is switched on as a linear function of a neuron’s firing rate.

We shall take the output firing rate function $f(J)$ to be a nonlinear sigmoid function of the input current J . One typical choice is the smooth sigmoidal firing rate function

$$f(J) = \frac{1}{1 + \exp(-\eta(J - \kappa))}, \quad (2.3)$$

with gain η and input threshold κ . Some progress has been made in analytically establishing links between model parameters and resultant solutions of neural field models with smooth sigmoidal firing rates (Kishimoto and Amari 1979; Faugeras et al. 2009; Pinto and Ermentrout 2001; Coombes and Schmidt 2010; Ermentrout et al. 2010).

In addition, we will study the effects of using a piecewise linear firing rate function

$$f(J) = \begin{cases} 0, & J \in (-\infty, \kappa), \\ \gamma(J - \kappa), & J \in (\kappa, \kappa + 1/\gamma), \\ 1, & J \in (\kappa + 1/\gamma, \infty), \end{cases} \quad (2.4)$$

with slope $0 < \gamma < \infty$ acting as a gain parameter in simulations of the model in Section 5. Piecewise linear

firing rate functions have been employed in some previous studies of neural fields with nonlinear adaptation, which has allowed analytic derivation of conditions for moving pulses (Hansel and Sompolinsky 1998) and self-sustained oscillations (Kilpatrick and Bressloff 2010b). We shall employ the sigmoid (2.3) and piecewise linear (2.4) functions with finite gain in simulations of the model in Section 5.

However, more analytical progress can be made on studying solutions of the networks (2.1) and (2.2) if the assumption of a smooth firing rate function is relaxed by taking f to be the high-gain limit $\eta \rightarrow \infty$ of the sigmoidal function (2.3) or $\gamma \rightarrow \infty$ of the piecewise linear function (2.4). Following Amari’s original work on scalar networks (Amari 1977), most analytical studies of the neural fields with negative feedback take the nonlinear firing-rate function f to be a Heaviside step function (Pinto and Ermentrout 2001; Folias and Bressloff 2004, 2005b; Troy and Shusterman 2007; Kilpatrick and Bressloff 2010b):

$$f(J) = H(J - \kappa) = \begin{cases} 0, & J \in (-\infty, \kappa), \\ 1, & J \in (\kappa, \infty). \end{cases} \quad (2.5)$$

We will use such a function in order to study the existence and stability of traveling waves, bumps, and the ON state (see Sections 3 and 4).

The strengths of connections between neurons in the network are specified by the weight function $w(x, x') = w(x - x')$, which is necessarily 2π -periodic in $x - x'$ since the domain is as well. Note that we are employing a model akin to the previously studied “ring” model of orientation preference in which synaptic weights are a function of the difference in orientation preferences, often selected as the sum of the two lowest order even harmonics (Ben-Yishai et al. 1995; Bressloff and Cowan 2002; York and van Rossum 2009). For our studies of trailing visual phenomena, the case that the size of the circle traced by the rotating is relatively small allows us to consider a periodic spatial domain $x \in (-\pi, \pi)$ and employ a function initially to study existence and stability of solutions in the network

$$w(x) = w_0 + w_2 \cos(x), \quad x \in (-\pi, \pi), \quad (2.6)$$

where w_0 is the mean strength of connectivity (or average network excitation since we restrict $w_0 > 0$) and w_2 is the modulation strength. To mimic alterations in the strengths of synaptic connections, we shall vary both of these parameters throughout our study. The weight function (2.6) is reasonable, so long as the circle traced by the rotating spot stimulus is sufficiently small, in other words as long as all neurons responding

to the stimulus are close enough to communicate. In this case, neurons that are close to one another will excite one another and distal neurons will inhibit one another, with lateral inhibition connectivity. Analysis of the networks (2.1) and (2.2) is straightforward in the case of the harmonic weight function (2.6). However, it is conceivable that the rotating spot stimulus applied to a subject may have a circular path that is wide enough that connection strengths between some patches of neurons are effectively zero. In this case, the size of the domain would increase and we take the weight function

$$w(x - x') = e^{-|x-x'|/\sigma_e} - A_i e^{-|x-x'|/\sigma_i}, \quad |x - x'| \in [0, L], \quad (2.7)$$

where A_i parametrizes the amount of synaptic inhibition, σ_e (σ_i) the spatial scale of excitatory (inhibitory) connections, and L the spatial size of the network. The analysis of Sections 3 and 4 could be extended to a system with the weight function (2.7). Resulting formulae would merely be more tedious to derive and not as straightforward to examine. Thus, we simply perform numerical simulations of the system with a larger spatial domain and weight function (2.7) in Section 5.

We specify the rotating input $I(x - ct)$ as being always non-negative and periodic upon the spatial domain $x \in (-L, L)$. A class of functions that fits this restriction is

$$I(x - ct) = I_0 \cos^2\left(\frac{x - ct}{2}\right) \quad (2.8)$$

where I_0 is the strength of this input, which we use for our analysis of the system in Sections 3 and 4. In the simulations of Section 5, where we extend our study to larger networks, we use a Gaussian input stimulus

$$I(x - ct) = I_0 e^{-(x-ct)^2/\sigma_I^2}, \quad (x - ct) \in [-L, L], \quad (2.9)$$

where I_0 is input strength, σ_I the input spatial scale, and the domain width $L > \pi$ for the simulations in which we use this input. For the bulk of the paper, we use stimulus strengths I_0 high enough so that substantial portions of the network operate close to saturation. This is in light of the fact that we are modeling high contrast visual inputs (see Fig. 1). Ben Yishai and colleagues examined the effects of weak inputs in a ring model without adaptation, where they could essentially exploit the fact that $I_0 \ll 1$ to perform perturbative analysis (Ben-Yishai et al. 1997). Our analysis will not rely on this weak input assumption.

Finally, to restrict some parameters of both models, we make the following observations. We consider synaptic time constants to be typically around 10 ms.

Therefore, by fixing the time constant of the u evolution equation to $\tau = 1$, we equate a single time unit with 10 ms. Therefore, since experimentally, the time constant of adaptation is considered to be between 40 and 120 ms (Madison and Nicoll 1984; Stocker et al. 1999), we should vary α roughly between 4 and 12.

3 Linear adaptation

We first consider the spatiotemporal dynamics arising in the network with linear adaptation (2.1) and explicitly compute existence and stability of various spatially structured solutions. In particular, we are concerned with the effect weight function parameters have on these solutions. First, we study spatially homogeneous solutions of the network, where input is spatially homogeneous and either time-invariant or time-periodic. Time-periodic stimuli are meant to model flickering light experiments (Abraham and Wolf 1988). Then, we proceed to studying spatially structured solutions that arise for finite stimulus rotation speed c . For sufficiently high speed c and input I_0 , we find the existence of an ON state, where the input drive $u(x, t) > \kappa$. For sufficiently weak excitation w_0 , we find there exists a critical value of c for which the ON state fails to exist. Then, either translationally invariant pulses or traveling breathers exist, depending on stability conditions, developed following an Evans function approach (Zhang 2004; Folias and Bressloff 2005b). Finally, when the stimulus speed is $c = 0$, we can carry out a greatly simplified analysis of existence and stability of bumps in the network as in Folias and Bressloff (2004) and Coombes and Owen (2004). Results are summarized in diagrams of parameter space which indicate transitions such as that from the ON state to stimulus-locked state. We find results of this network match the prediction that for sufficiently elevated synaptic modulation w_2 in a network, trailing phenomena are induced much more easily.

3.1 Space-clamped system

To examine fundamental effects of varying the different parameters of the model, especially those related to adaptation, it is useful to study a space-clamped version of the full set of equations, which essentially assumes spatially homogeneous solutions can arise as long as $I(x, t) = I(t)$ is itself spatially homogeneous. Shusterman and Troy carried out such an analysis in the case without input, finding limit cycles arise for a critical large value of β (Shusterman and Troy 2008). We will study the system with linear adaptation in two different

situations, both of which reduce the integrodifferential equations (2.1) to a pair of ordinary differential equations

$$\begin{aligned} \dot{u} &= -u - v + \bar{w}H(u - \kappa) + I(t), \\ \alpha\dot{v} &= -v + \beta u, \end{aligned} \tag{3.1}$$

where u and v are now only functions of t . In the first situation, we examine Eq. (2.1) in the limit of infinite rotation speed $c \rightarrow \infty$ so that Eq. (2.8) becomes

$$I(t) = \bar{I} = \lim_{c \rightarrow \infty} I(x - ct) = I_0 \int_{-\pi}^{\pi} \cos^2\left(\frac{x}{2}\right) dx = \pi I_0,$$

and the synaptic weight function’s effect can be reduced, in the case of the harmonic weight (2.6) and $L = \pi$, to

$$\bar{w} = \int_{-\pi}^{\pi} w_0 + w_2 \cos x dx = 2\pi w_0.$$

Now in order to identify homogeneous solutions of the full system (2.1), we need only identify fixed points of the system (3.1), which are given by the pair of equations

$$u_0 = \frac{\bar{w}}{1 + \beta} H(u_0 - \kappa) + \bar{I}, \tag{3.2}$$

$$v_0 = \beta u_0. \tag{3.3}$$

We can solve explicitly for all fixed points and provide conditions for their existence

$$u_0 = \frac{\bar{w}}{1 + \beta} + \bar{I}, \quad v_0 = \frac{\beta\bar{w}}{1 + \beta} + \beta\bar{I}, \quad \text{exists if } \frac{\bar{w}}{1 + \beta} + \bar{I} > \kappa,$$

$$u_0 = \bar{I}, \quad v_0 = \beta\bar{I} \quad \text{exists if } \bar{I} < \kappa,$$

and notice a maximum of two fixed points exist in this case. This is due to the fact that there is a jump discontinuity in the firing rate function. The eigenvalues corresponding to the linear stability of both equilibria are

$$\lambda_{\pm} = \frac{1}{2} \left[-(1 + \alpha^{-1}) \pm \sqrt{(1 - \alpha^{-1})^2 - 4\beta\alpha^{-1}} \right], \tag{3.4}$$

so both equilibria are always stable. There is still a separatrix in phase space between the basins of attraction of these two points, but there is no fixed point upon it; this is where the system is discontinuous. Thus, when the firing rate function is a Heaviside (2.5), the full system (2.1) will support only the ON state if $\bar{I} > \kappa$ (implying $\bar{w}/(1 + \beta) + \bar{I} > \kappa$, since $\bar{w} \geq 0$), only the OFF state if $\bar{w}/(1 + \beta) + \bar{I} < \kappa$, and both ON and OFF states if $\bar{I} < \kappa$ but $\bar{w}/(1 + \beta) + \bar{I} > \kappa$. In the bistable case, there is not enough drive to the system to force activity ON from rest, but enough recurrent excitation to keep the activity ON once the system is switched on with a perturbation. We illustrate these possibilities in Fig. 2. Note that it is also possible for the system (3.1) to exhibit self-sustained oscillations for sufficiently large β , as was shown in Shusterman and Troy (2008). However, we are not concerned with this case since it is not indicative of a particular visual symptom of HPPD. In the following subsections, we find the state of the system undergoes a series of bifurcations as c is reduced from infinity so the solution goes from a homogeneous ON state, to an inhomogeneous ON state, to a breathing and/or stimulus-locked pulse, and finally to a stationary bump.

The second situation we study is that corresponding to the input of a flashing light to the network (2.1). This corresponds to a spatially homogeneous, but time-periodic input

$$I(x, t) = I(t) = I_0 H(\sin(\pi t/T_I)), \tag{3.5}$$

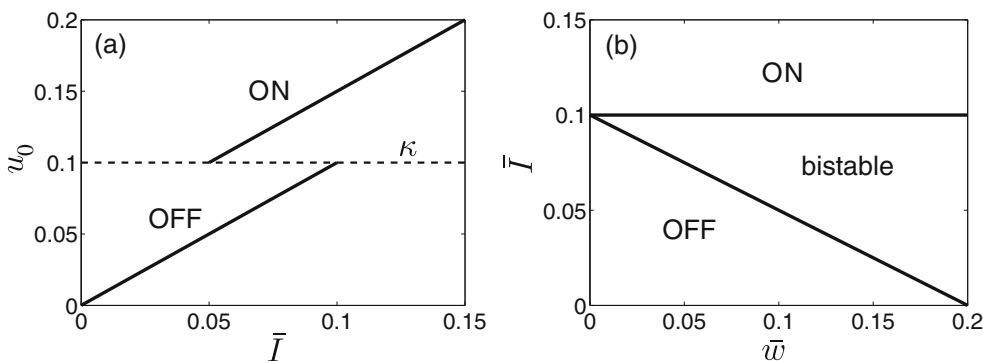


Fig. 2 Equilibria of the space-clamped system (3.1). **(a)** Plot of the equilibrium values of u as the level of input to the network \bar{I} is varied. The net level of excitation is fixed $\bar{w} = 0.1$. As \bar{I} is increased from zero, the system transitions from having only the

OFF state, to being bistable, to strictly having an ON state. **(b)** Phase diagram of system states in (\bar{w}, \bar{I}) space. Other parameters are $\kappa = 0.1$ and $\beta = 1$

so that $I = I_0$ when $t \in (2nT_I, (2n + 1)T_I)$ and $I = 0$ when $t \in ((2n + 1)T_I, 2(n + 1)T_I)$ for $n \in \mathbb{Z}$. We would expect the system to become entrained to the input signal $I(t)$, resulting in a time-periodic solution with period $2T_I$. Our study of this system is motivated by experiments showing that patients with HPPD begin seeing a fusion of light at a lower flicker frequency than control groups (Abraham and Wolf 1988). Thus, we will examine the effect that increasing net excitation \bar{w} has upon the critical frequency $\omega^* = 1/2T_I^*$ at which the network is indefinitely in an ON, or superthreshold, state. To do this, we shall first solve the system (3.1) under the assumption that the flicker period $2T_I$ is low enough and the input strength I_0 is high enough such that the system is always ON. In this case, assuming the system has settled into the attracting oscillation, we can solve the system to find over a single period

$$u(t) = \frac{\bar{w} + I_0}{1 + \beta} + \frac{I_0}{2\mathcal{B}(1 + \beta)} \times \left[\frac{(A - \mathcal{B})e^{\lambda_+ t}}{e^{\lambda_+} + 1} - \frac{(A + \mathcal{B})e^{\lambda_- t}}{e^{\lambda_-} + 1} \right] : t \in [0, T_I],$$

$$u(t) = \frac{\bar{w}}{1 + \beta} + \frac{I_0}{2\mathcal{B}(1 + \beta)} \times \left[\frac{(A + \mathcal{B})e^{\lambda_- t}}{e^{\lambda_- T_I} + 1} - \frac{(A - \mathcal{B})e^{\lambda_+ t}}{e^{\lambda_+} + 1} \right] : t \in [T_I, 2T_I],$$

where the eigenvalues λ_{\pm} are given by Eq. (3.4), and

$$A = \alpha + 2\alpha\beta - 1,$$

$$\mathcal{B} = \sqrt{\alpha^2 + 1 - 2\alpha - 4\alpha\beta}.$$

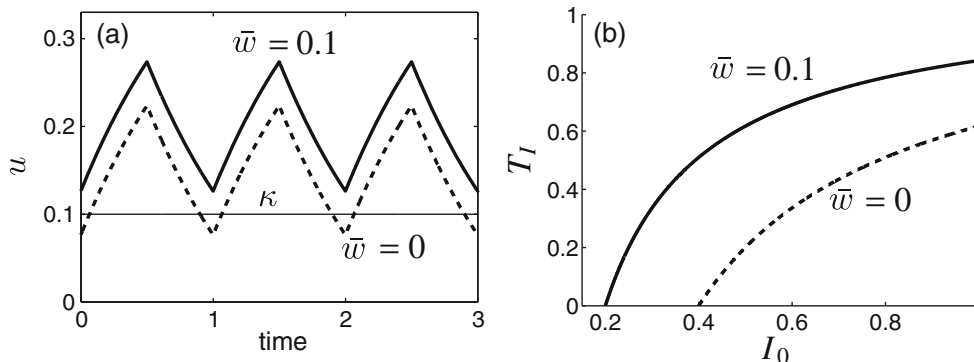


Fig. 3 (a) Evolution of u in time when subject to a flicker stimulus specified by Eq. (3.5) where $T_I = 0.5$ and $I_0 = 0.6$ for $\bar{w} = 0$ (dashed) and $\bar{w} = 0.1$ (solid). Notice that for elevated excitation ($\bar{w} = 0.1$), the input current remains superthreshold ($u > \kappa$) for the entirety of the stimulus period $2T_I = 1$, while the network with less excitation ($\bar{w} = 0$) does not. (b) Plot of the critical value

of T_I versus input strength I_0 determined by Eq. (3.6) for $\bar{w} = 0$ (dashed) and $\bar{w} = 0.1$ (solid). Above these curves, the input current u is not always superthreshold, but represents a flicker. Below these curves the input current is always superthreshold, representing a fusion state. Other parameters are $\kappa = 0.1$, $\alpha = 10$, and $\beta = 1$

$$\frac{\bar{w}}{1 + \beta} + \frac{I_0}{2\mathcal{B}(1 + \beta)} \left[\frac{A + \mathcal{B}}{1 + e^{-\lambda_- T_I}} - \frac{A - \mathcal{B}}{1 + e^{-\lambda_+ T_I}} \right] = \kappa. \tag{3.6}$$

We plot curves given by Eq. (3.6), partitioning parameter space into regions where fusion exists and where flickering is actually perceived in Fig. 3, also depicting the effect of increased net excitation on the evolution of neural activity. Notice the network with more excitation maintains fusion where the network with less does not.

3.2 Loss of the ON state

We now proceed by studying the loss of the existence of the ON state as the speed of the constant strength stimulus c is reduced from infinity. In keeping with the phenomenon we are modeling, we will presume that we are in a regime where the system does not support the ON state in the case that $\bar{I} = 0$, so $\bar{w} < (1 + \beta)\kappa$. Also, we continue to consider the case of a Heaviside firing rate function (2.5), since we can develop analytic expressions relating parameters to existence regions of certain dynamics. We shall study the case of a smooth sigmoidal firing rate in numerical simulations of Section 5.

To start, consider the full network with linear adaptation (2.1) with the simple sum of harmonics weight

function (2.6), on the spatial domain $x \in (-\pi, \pi)$, and rotating input with finite speed, so

$$\begin{aligned}
 u_t &= -u - v + \int_{-\pi}^{\pi} (w_0 + w_2 \cos(x - x')) \\
 &\quad \times H(u(x', t) - \kappa) dx' + I_0 \cos^2\left(\frac{x - ct}{2}\right), \\
 v_t &= (-v + \beta u) / \alpha.
 \end{aligned}
 \tag{3.7}$$

In order to check if the ON state exists for particular choice of input, we use a constructive approach. First, assume such a solution does exist, so that the network is ON ($u(x, t) > \kappa$) at all values $x \in (-\pi, \pi)$ for all time t . In addition, we make a change of coordinates to a rotating frame $\xi = x - ct$, so the set of Eq. (3.7) becomes

$$\begin{aligned}
 -cU'(\xi) &= -U(\xi) - V(\xi) \\
 &\quad + \int_{-\pi}^{\pi} (w_0 + w_2 \cos(\xi - \xi')) d\xi' + I_0 \cos^2 \frac{\xi}{2}, \\
 -cV'(\xi) &= (-V(\xi) + \beta U(\xi)) / \alpha.
 \end{aligned}
 \tag{3.8}$$

It is straightforward to solve this system by converting it to a single second order differential equation

$$\begin{aligned}
 -c^2U''(\xi) + c(1 + \alpha^{-1})U'(\xi) - \alpha^{-1}(1 + \beta)U(\xi) \\
 = -\frac{2\pi w_0}{\alpha} - \frac{I_0}{2} \left[c \cdot \sin \xi + \frac{\cos \xi + 1}{\alpha} \right].
 \end{aligned}
 \tag{3.9}$$

Along with periodic boundary conditions $U(-\pi) = U(\pi)$ and $V(-\pi) = V(\pi)$, solving Eq. (3.9) for U and using Eq. (3.8) to generate V gives

$$U(\xi) = \frac{2\pi w_0 + I_0/2}{1 + \beta} - \mathcal{U}_1 \sin \xi + \mathcal{U}_2 \cos \xi,
 \tag{3.10}$$

$$V(\xi) = \frac{\beta(2\pi w_0 + I_0/2)}{1 + \beta} - \mathcal{V}_1 \sin \xi + \mathcal{V}_2 \cos \xi,
 \tag{3.11}$$

where

$$\begin{aligned}
 \mathcal{U}_1 &= \frac{I_0(\alpha^2 c^3 + c - \alpha c \beta)}{2\mathcal{D}}, \\
 \mathcal{U}_2 &= \frac{I_0(\alpha^2 c^2 + 1 + \beta)}{2\mathcal{D}},
 \end{aligned}$$

with

$$\mathcal{D} = c^2(\alpha + 1)^2 + (\alpha c^2 - (1 + \beta))^2,$$

and

$$\begin{aligned}
 \mathcal{V}_1 &= \frac{\beta I_0 c(\alpha + 1)}{2\mathcal{D}}, \\
 \mathcal{V}_2 &= \frac{\beta I_0(1 + \beta - \alpha c^2)}{2\mathcal{D}}.
 \end{aligned}$$

Therefore, in order that the ON state exist for a particular set of parameters, we require that the input drive be superthreshold everywhere in the domain, that is $U(\xi) > \kappa$ for all $\xi \in (-\pi, \pi)$. We can ensure this restriction holds by requiring that simply the minimum of U be superthreshold, $U(\xi_m) > \kappa$, which yields the following inequality

$$U(\xi_m) = \frac{2\pi w_0 + I_0/2}{1 + \beta} - \sqrt{\mathcal{U}_1^2 + \mathcal{U}_2^2} > \kappa,$$

or

$$\begin{aligned}
 \frac{2\pi w_0 + I_0/2}{1 + \beta} \\
 - \frac{I_0 \sqrt{(\alpha^2 c^3 + c - \alpha c \beta)^2 + (\alpha^2 c^2 + 1 + \beta)^2}}{2(c^2(\alpha + 1)^2 + (\alpha c^2 - (1 + \beta))^2)} > \kappa,
 \end{aligned}
 \tag{3.12}$$

constraining parameters for the ON state to exist. Notice that in the limit of an infinite speed stimulus, the inequality (3.12) becomes the restriction imposed by our calculations using the space-clamped system

$$\lim_{c \rightarrow \infty} U(\xi_m) = \frac{2\pi w_0 + I_0/2}{1 + \beta} > \kappa.
 \tag{3.13}$$

Presuming then that the ON state exists for infinite c , we can identify the critical stimulus speed value c_* at which the ON state ceases to exist as that for which the inequality (3.12) becomes a strict equality

$$\begin{aligned}
 \frac{2\pi w_0 + I_0/2}{1 + \beta} \\
 - \frac{I_0 \sqrt{(\alpha^2 c_*^3 + c_* - \alpha c_* \beta)^2 + (\alpha^2 c_*^2 + 1 + \beta)^2}}{2(c_*^2(\alpha + 1)^2 + (\alpha c_*^2 - (1 + \beta))^2)} = \kappa.
 \end{aligned}$$

We plot the relationship between c_* and the strength of the input I_0 in Fig. 4 for a wide range of input strengths, showing the boundary between an ON state existing and not existing. Notice that this critical value c_* is higher in the network with less net excitation. LSD may lead to a net increase in the strength of excitatory connections in networks that process visual inputs (Nichols and Sanders-Bush 2002). Our results suggest this may lead to excessive broadening of the network signal representing a moving input, which could be interpreted as a halo in the context of HPPD (Abraham 1983). To illustrate the behavior of the ON state, we show a plot of the solution for a value of c slightly above c_* for a particular value of I_0 .

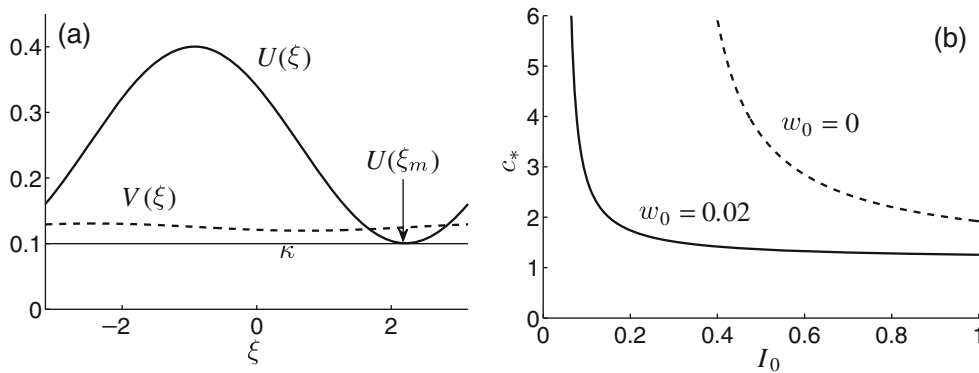


Fig. 4 (a) The ON state plotted for stimulus speed $c = 1.37$, slightly above the critical speed for the stimulus strength $I_0 = 0.5$ and net excitation $w_0 = 0.02$. The minimum $U(\xi_m)$ lies slightly

above the threshold κ . (b) Critical value of c_* calculated using Eq. (3.12) plotted versus stimulus strength I_0 for threshold $\kappa = 0.1$. Other parameters are $\alpha = 10$, $\beta = 0.5$, and $w_2 = 0.5$

3.3 Stimulus-locked pulses

Few studies of neural field models have examined the effects of a propagating input. In a ring model with nonlocal inhibition rather than local adaptation, Ben Yishai and colleagues performed a study of the ability of a network to lock to a propagating input (Ben-Yishai et al. 1997). Folias and Bressloff explored the existence and stability of stimulus-locked pulses in a network with linear adaptation on the infinite domain with a Heaviside firing rate (Folias and Bressloff 2005b). Also, more recently a similar study was carried out in a network with a smooth firing rate function in Ermentrout et al. (2010). Our work here diverges from those studies as it is set on a periodic domain and operates in parameter ranges where the leading and trailing edges of the pulse will interact. Since we have a weight function in our model with inhibition, we find that when instabilities of the stimulus-locked pulses arise, the breathing solutions that result are lurching rather than simply expanding and contracting. This is actually more indicative of the phenomenon of discrete afterimages seen during visual trails (Abraham 1983; Kawasaki and Purvin 1996; Dubois and VanRullen 2011).

3.3.1 Existence

Therefore, we proceed by looking for stimulus-locked traveling pulse solutions to the network with linear adaptation (2.1) and Heaviside firing rate function (2.5). Considering traveling pulse solutions with width Δ , we again employ the traveling wave coordinate $\xi = x - ct$ and define the superthreshold region $\xi \in (\pi - \Delta, \pi)$, where we can arbitrarily select the leading edge’s location due to underlying translation invariance of the problem. Additionally, we must specify a spatial shift

for the input, such that $I(x, t) = I_0 \cos^2((\xi + \Delta_I)/2)$. Thus, we have the following set of equations defining a stimulus-locked traveling pulse solution

$$\begin{aligned}
 -cU'(\xi) &= -U(\xi) - V(\xi) + \int_{\pi-\Delta}^{\pi} w_0 + w_2 \cos(\xi - \xi') d\xi' \\
 &\quad + I_0 \cos^2\left(\frac{\xi + \Delta_I}{2}\right), \\
 -cV'(\xi) &= (-V(\xi) + \beta U(\xi))/\alpha.
 \end{aligned}
 \tag{3.14}$$

We may also solve this system by first converting it to a single second order differential equation

$$\begin{aligned}
 -c^2U''(\xi) + c(1 + \alpha^{-1})U'(\xi) - \alpha^{-1}(1 + \beta)U(\xi) \\
 &= -\frac{w_0\Delta}{\alpha} - \frac{I_0}{2\alpha} + \frac{w_2}{\alpha}(\sin(\Delta + \xi) - \sin \xi) \\
 &\quad + cw_2(\cos \xi - \cos(\Delta + \xi)) - \frac{cI_0}{2} \sin(\xi + \Delta_I) \\
 &\quad - \frac{I_0}{2\alpha} \cos(\xi + \Delta_I).
 \end{aligned}
 \tag{3.15}$$

Along with the periodic boundary conditions $U(-\pi) = U(\pi)$ and $V(-\pi) = V(\pi)$, solving Eq. (3.15) for U and using Eq. (3.14) to generate V yields

$$\begin{aligned}
 U(\xi) &= \frac{w_0\Delta + I_0/2}{1 + \beta} \\
 &\quad + \mathcal{U}_3 \left[w_2 \sin \xi - w_2 \sin(\xi + \Delta) + \frac{I_0}{2} \cos(\xi + \Delta_I) \right] \\
 &\quad + \mathcal{U}_4 \left[w_2 \cos \xi - w_2 \cos(\xi + \Delta) - \frac{I_0}{2} \sin(\xi + \Delta_I) \right],
 \end{aligned}
 \tag{3.16}$$

$$\begin{aligned}
 V(\xi) = & \frac{\beta(w_0\Delta + I_0/2)}{1 + \beta} \\
 & + \mathcal{V}_3 \left[w_2 \sin(\xi + \Delta) - w_2 \sin \xi - \frac{I_0}{2} \cos(\xi + \Delta_I) \right] \\
 & + \mathcal{V}_4 \left[w_2 \cos \xi - w_2 \cos(\xi + \Delta) - \frac{I_0}{2} \sin(\xi + \Delta_I) \right],
 \end{aligned}
 \tag{3.17}$$

where

$$\begin{aligned}
 \mathcal{U}_3 &= \frac{\alpha^2 c^2 + 1 + \beta}{\mathcal{D}}, \\
 \mathcal{U}_4 &= \frac{\alpha^2 c^3 - \alpha c \beta + c}{\mathcal{D}},
 \end{aligned}$$

and

$$\begin{aligned}
 \mathcal{V}_3 &= \frac{\alpha c^2 \beta - \beta(1 + \beta)}{\mathcal{D}}, \\
 \mathcal{V}_4 &= \frac{\beta c(\alpha + 1)}{\mathcal{D}}.
 \end{aligned}$$

Therefore, to specify the pulse width Δ and associated shift to the input Δ_I , we impose self consistency by requiring that the input current $U(\xi)$ specified by Eq. (3.16) cross firing threshold κ at the leading and trailing edge of the pulse such that $U(\pi) = U(\pi - \Delta) = \kappa$. This generates the following nonlinear system of equations

$$\begin{aligned}
 \frac{w_0\Delta + I_0/2}{1 + \beta} + \mathcal{U}_3 \left[w_2 \sin \Delta - \frac{I_0}{2} \cos \Delta_I \right] \\
 + \mathcal{U}_4 \left[w_2(\cos \Delta - 1) + \frac{I_0}{2} \sin \Delta_I \right] = \kappa,
 \end{aligned}$$

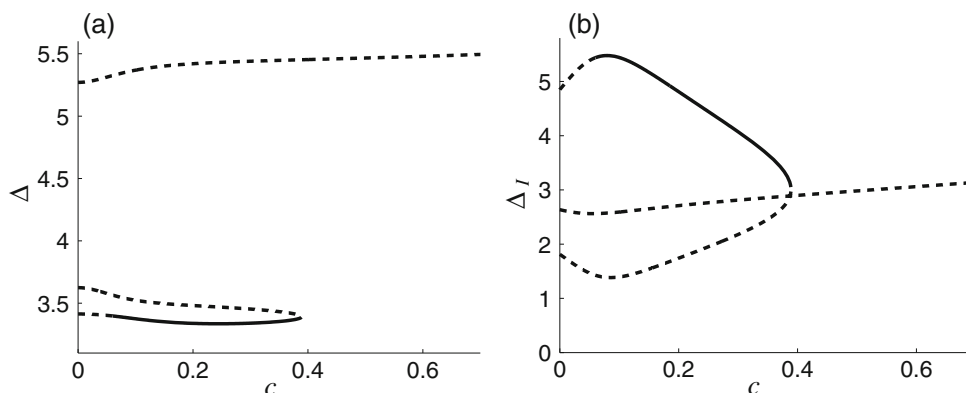


Fig. 5 Dependence of the (a) pulsewidth Δ and (b) input shift Δ_I on the stimulus speed c . For sufficiently slow inputs, there are three traveling pulse solutions, two unstable (*dashed*), one stable (*solid*). At a critical value of c , two solutions annihilate

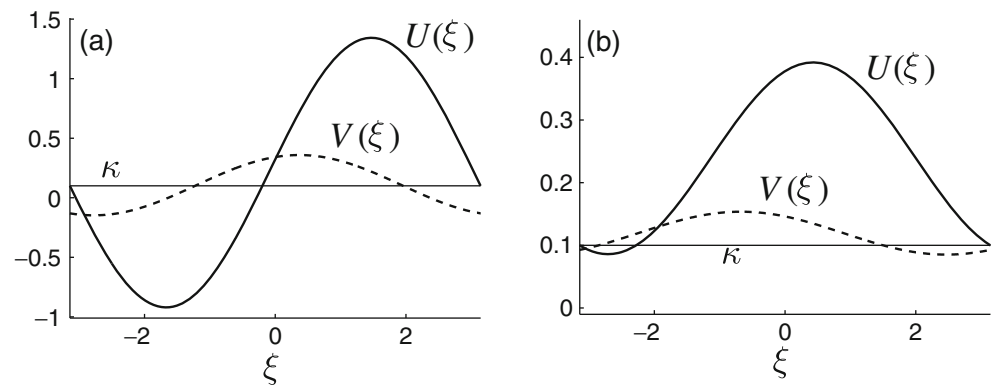
$$\begin{aligned}
 \frac{w_0\Delta + I_0/2}{1 + \beta} + \mathcal{U}_3 \left[w_2 \sin \Delta - \frac{I_0}{2} \cos(\Delta_I - \Delta) \right] \\
 + \mathcal{U}_4 \left[w_2(1 - \cos \Delta) + \frac{I_0}{2} \sin(\Delta_I - \Delta) \right] = \kappa,
 \end{aligned}$$

which can be solved numerically.

We show the dependence of pulse width Δ and input shift Δ_I on stimulus speed c in Fig. 5. Example profiles of a stable and an unstable pulse are pictured in Fig. 6. The results shown are representative of the qualitative behavior of stimulus-driven traveling pulses for a wide range of parameters. There is an intermediate range of stimulus speeds for which a stable traveling pulse is the attracting solution, but this branch can become unstable for very slow stimuli. This reflects the speed of intrinsic traveling pulses that exist in the network when no inputs are present (Ben-Yishai et al. 1997; Folias and Bressloff 2005b). There are two other unstable pulse solutions as well. We present our calculation of stability in the following subsection. As the stimulus speed is increased, at a critical value of c , the stable branch annihilates with an unstable branch while the other unstable branch persists. When the stimulus speed is beyond this critical value, there will be no translationally invariant traveling pulses. Thus, we associated the onset of trailing phenomena with this critical value of c , as long as it is less than the speed necessary for the ON state to exist. The location of this point depends quite weakly on net excitation w_0 , and more strongly on the overall modulation of synaptic connectivity w_2 , decreasing monotonically as w_2 is increased. The partitioning of parameter space into the stable solutions existing is shown in Fig. 7 for both (w_2, c) and (I_0, c) . Notice, for sufficiently weak synaptic strength modulation,

one another and a single unstable solution remains. Stability is determined by the zeros of the Evans function $\mathcal{E}(\lambda) = |\mathcal{A}_p - I|$ where \mathcal{A}_p is given by Eq. (3.21). Other parameters are $\kappa = 0.1$, $\alpha = 10$, $\beta = 0.5$, $w_0 = 0.02$, $w_2 = 0.5$, and $I_0 = 0.5$

Fig. 6 Profiles of the (a) stable and (b) upper unstable pulse solutions $U(\xi)$ and $V(\xi)$ given by Eqs. (3.16) and (3.17), respectively, when $c = 0.2$. Note that the solution remains above threshold within the region $\xi \in (\pi - \Delta, \pi)$. Other parameters are $\kappa = 0.1$, $\alpha = 10$, $\beta = 0.5$, $w_0 = 0.02$, $w_2 = 0.5$, and $I_0 = 0.5$



there are no c values for which traveling breathers exist, and there is a region of bistability where stable locked pulses and the ON state exist. It appears that the lower range of w_2 provides physiologically reasonable results in our idealized model, and more unfaithful representations of stimuli arise as modulation increases. Therefore, our model predicts that visual trails may arise from an overall strengthening of both excitatory and inhibitory connections through some modulation of neurotransmitter concentration. Numerical simulations of different scenarios of stimulus-driven pulses, as the stimulus speed increases, are pictured in Fig. 8. This reflects the analytically predicted behavior calculated using stability analysis in the next subsection.

3.3.2 Stability

We now calculate the stability of the above stimulus locked pulse solutions. As was shown by Folias and Bressloff (2005b), stimulus-locked pulses in a network

with linear adaptation can lose stability through a Hopf bifurcation, resulting in traveling breathers. In the context of neural substrates of visual experience, traveling breathers would imply a subject witnessing haloes around or afterimages behind the traveling spot stimulus. This has been seen in several studies of exhallucinogen users (Abraham 1983; Halpern and Pope 2003; Dubois and VanRullen 2011). Therefore, we proceed by examining the onset of such solutions using a linear stability analysis of the spatially structured solutions derived in the previous section.

We begin by examining the evolution of small, smooth perturbations to the traveling pulse solution $(U(\xi), V(\xi))$. Common to such stability calculations, we assume the perturbations are separable in time and the wave coordinate such that $u(\xi, t) = U(\xi) + e^{\lambda t} \psi(\xi)$ and $v(\xi, t) = V(\xi) + e^{\lambda t} \phi(\xi)$ (Coombes and Owen 2004; Folias and Bressloff 2005b). In addition, we require that $e^{\lambda t}(\psi(\xi), \phi(\xi))$ are sufficiently small such that Taylor series expansions are valid. Thus, our

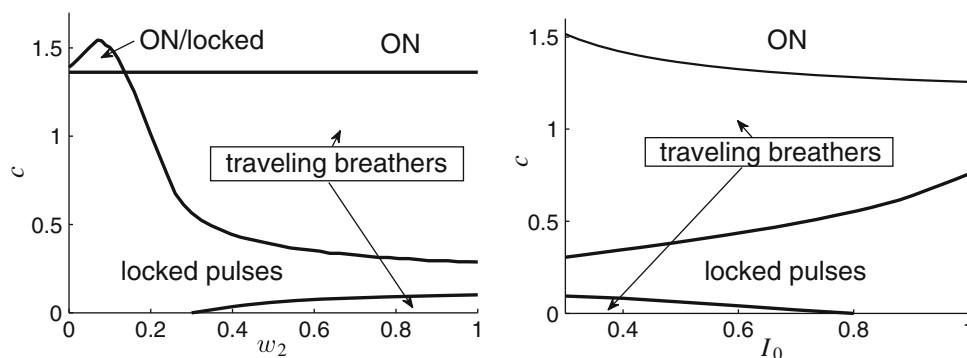


Fig. 7 (a) Partition of (w_2, c) parameter space, where $I_0 = 0.5$, into four different regimes. Very slow stimuli are not tracked for high enough synaptic modulation w_2 . Above this range, slow enough stimuli are tracked as a translationally invariant traveling pulse. As the stimulus speed increases, there is a critical value of c beyond which the invariant solution slips off of the stimulus, leading to traveling breathers. This corresponds to discrete after-

images at each slip time. For very fast stimuli, the ON state exists, corresponding to the whole domain being superthreshold. For weak synaptic strength modulation w_2 , the signal is either tracked as a locked pulse or the whole domain is superthreshold, and a region of bistability exists. (b) Partition of (I_0, c) parameter space for $w_2 = 0.5$. Other parameters are $\kappa = 0.1$, $\alpha = 10$, $\beta = 0.5$, and $w_0 = 0.02$

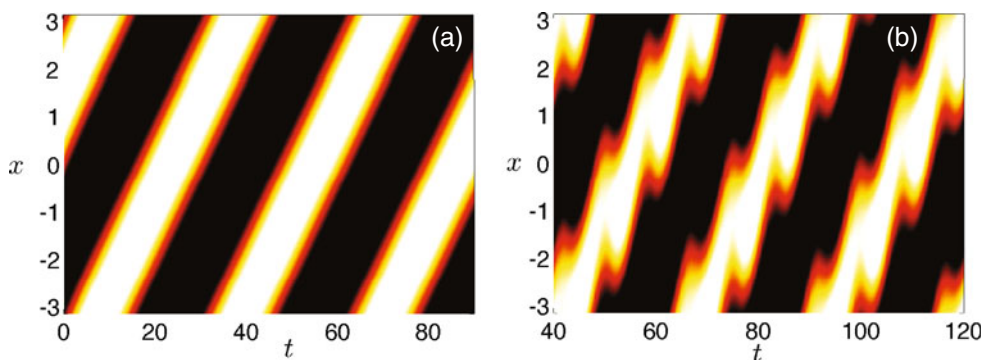


Fig. 8 Numerical simulations of stimulus-locked pulses and traveling breathers in the network with linear adaptation (2.1) for a Heaviside firing rate (2.5), where $u(x, t)$ is plotted. **(a)** For a speed ($c = 0.2$) within the region of parameter space where stable locked traveling pulses exist. **(b)** For a speed ($c = 1$) beyond the

critical speed where stable pulses cease to exist, superthreshold activity periodically lurches, representative of a discrete afterimage. Other parameters are $\kappa = 0.1$, $\alpha = 10$, $\beta = 0.5$, $w_0 = 0.02$, $w_2 = 0.5$, and $I_0 = 0.5$

analysis proceeds by plugging these expressions in the system (2.1) along with the traveling pulse solutions (3.16) and (3.17). Upon expanding to first order in (ψ, ϕ) , we arrive at the linear equation

$$\begin{aligned}
 -c\psi' + (\lambda + 1)\psi + \phi &= \frac{w(\xi - \pi)\psi(\pi)}{|U'(\pi)|} \\
 &\quad + \frac{w(\xi - \pi + \Delta)\psi(\pi - \Delta)}{|U'(\pi - \Delta)|}, \\
 -\phi' + (\lambda + \alpha^{-1})\phi &= \frac{\beta\psi}{\alpha}, \tag{3.18}
 \end{aligned}$$

where we have used the identity

$$\frac{dH(U(\xi) - \kappa)}{dU} = \frac{\delta(\xi - \pi)}{|U'(\pi)|} + \frac{\delta(\xi - \pi + \Delta)}{|U'(\pi - \Delta)|}. \tag{3.19}$$

In Folias and Bressloff (2005b), there is a detailed analysis of the complete spectrum of a similar linear operator on the infinite domain. We forgo such analysis here and focus particularly on the point spectrum of the operator in the system (3.18). In doing so, we can associate the point spectrum of the linear operator with the zeros of a complex analytic function called the Evans function (Coombes and Owen 2004). Thus, to predict the stability of stimulus-locked pulses, we look for nontrivial solutions of the eigenvalue problem (3.18). First, we note that the values which bound the essential spectrum $\lambda = -1 + ip$ and $\lambda = -\alpha^{-1} + ip$ ($p \in \mathbb{R}$) will not contribute to any instabilities. Omitting these values from the remainder of our analysis, we proceed by solving for the associated eigenfunctions. As we did in the solution of the existence problem, we

can solve for ϕ in terms of ψ to convert the system (3.18) to the following equation

$$\begin{aligned}
 -c\psi'' + ((c + 1)\lambda + c(1 + \alpha^{-1}))\psi' \\
 -((\lambda + \alpha^{-1})(\lambda + 1) + \beta\alpha^{-1})\psi \\
 &= \frac{\psi(\pi)}{|U'(\pi)|} [cw'(\xi - \pi) - (\lambda + \alpha^{-1})w(\xi - \pi)] \\
 &\quad + \frac{\psi(\pi - \Delta)}{|U'(\pi - \Delta)|} \\
 &\quad \times [cw'(\xi - \pi + \Delta) - (\lambda + \alpha^{-1})w(\xi - \pi + \Delta)].
 \end{aligned}$$

By treating the pointwise terms $\psi(\pi)$ and $\psi(\pi - \Delta)$ as constants, we can solve this equation as an inhomogeneous second order differential equation in the case of the harmonic weight function (2.6). Upon applying periodic boundary conditions, we arrive at the following expression for the eigenfunction

$$\begin{aligned}
 \psi(\xi) &= \left[\mathcal{P}_0 + \frac{\mathcal{P}_1 \sin \xi - \mathcal{P}_2 \cos \xi}{\mathcal{D}_p} \right] \frac{\psi(\pi)}{|U'(\pi)|} \\
 &\quad + \left[\mathcal{P}_0 + \frac{\mathcal{P}_1 \sin(\xi + \Delta) - \mathcal{P}_2 \cos(\xi + \Delta)}{\mathcal{D}_p} \right] \\
 &\quad \times \frac{\psi(\pi - \Delta)}{|U'(\pi - \Delta)|}, \tag{3.20}
 \end{aligned}$$

where

$$\begin{aligned}
 \mathcal{P}_0 &= \frac{w_0(\alpha\lambda + 1)}{\mathcal{A}_1}, \\
 \mathcal{P}_1 &= w_2[\alpha^2 c^3 - \alpha c \mathcal{A}_1 + c(\alpha\lambda + 1)\mathcal{A}_2], \\
 \mathcal{P}_2 &= w_2[(\alpha\lambda + 1)(\mathcal{A}_1 - \alpha c^2) + \alpha c^2 \mathcal{A}_2],
 \end{aligned}$$

with

$$A_1 = (\alpha\lambda + 1)(\lambda + 1) + \beta,$$

$$A_2 = 2\alpha\lambda + \alpha + 1,$$

$$D_p = [\alpha c^2 - A_1]^2 + (cA_2)^2.$$

Requiring self-consistency of the solution (3.20), we generate the following 2×2 linear system of equations $\psi = A_p \psi$ where

$$\psi = \begin{pmatrix} \psi(\pi) \\ \psi(\pi - \Delta) \end{pmatrix}, \quad A_p = \begin{pmatrix} A_{\pi\pi} & A_{\pi\Delta} \\ A_{\Delta\pi} & A_{\Delta\Delta} \end{pmatrix}, \quad (3.21)$$

with

$$A_{\pi\pi} = \frac{D_p \mathcal{P}_0 + \mathcal{P}_2}{D_p |U'(\pi)|},$$

$$A_{\pi\Delta} = \frac{D_p \mathcal{P}_0 - \mathcal{P}_1 \sin \Delta + \mathcal{P}_2 \cos \Delta}{D_p |U'(\pi - \Delta)|},$$

$$A_{\Delta\pi} = \frac{D_p \mathcal{P}_0 + \mathcal{P}_1 \sin \Delta + \mathcal{P}_2 \cos \Delta}{D_p |U'(\pi)|},$$

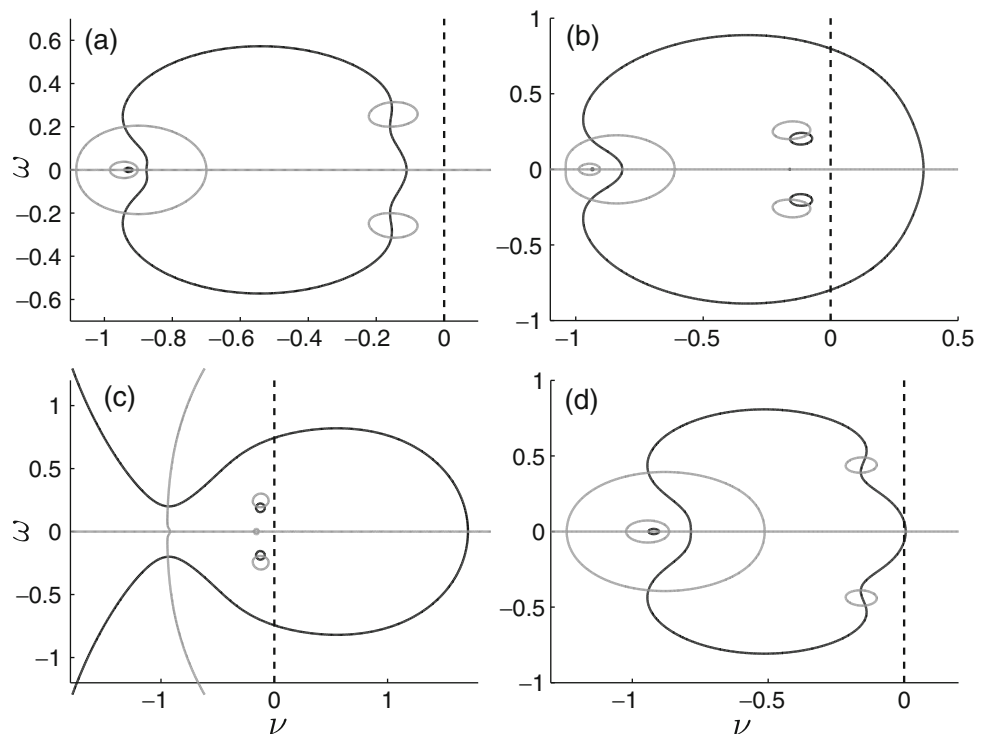
$$A_{\Delta\Delta} = \frac{D_p \mathcal{P}_0 + \mathcal{P}_2}{D_p |U'(\pi - \Delta)|}.$$

Then, continuing the approach of previous studies of the stability of traveling waves in neural fields (Zhang 2004; Coombes and Owen 2004; Folias and Bressloff 2005b), we look for nontrivial solutions of $\psi = A_p \psi$

such that $\mathcal{E}(\lambda) = 0$, where $\mathcal{E}(\lambda) = \det(A_p - I)$ is the Evans function of the traveling pulse solution (3.16) and (3.17). Since there are no other parts of the spectrum that would contribute to instabilities, the traveling pulse will be linearly stable as long as $\text{Re } \lambda < 0$ for all λ such that $\mathcal{E}(\lambda) = 0$. We can find the zeros of the Evans function by following (Coombes and Owen 2004) and writing $\lambda = \nu + i\omega$ and plotting the zero contours of $\text{Re}(\mathcal{E}(\lambda))$ and $\text{Im}(\mathcal{E}(\lambda))$ in the (ν, ω) -plane. The Evans function is zero where the lines intersect.

We present an example of this calculation for the traveling pulse solutions of Fig. 5. The upper unstable pulse has a positive real eigenvalue and the stable pulse’s eigenvalues are complex with negative real part according to the predictions of their zero contours in Fig. 9. Therefore, when c moves beyond the interval of existence for the stable pulse, we expect a translationally invariant traveling pulse to cease to exist. Only an unstable traveling pulse remains, and for a wide range of parameters, this is a breathing pulse. Previous studies of stimulus-driven neural fields show breathing pulses can arise through a Hopf bifurcation in the linear stability of the pulse, associated with complex eigenvalues with positive real part (Folias and Bressloff 2005b; Coombes and Owen 2005). Here, we find the breathing pulses in this network arise when a stable pulse solution annihilates with an unstable pulse,

Fig. 9 Evans function for the stimulus-locked traveling pulses (3.16) and (3.17) whose width Δ and shift Δ_I are plotted in Fig. 5. Zero contours of $\text{Re } \mathcal{E}(\lambda)$ (black) and $\text{Im } \mathcal{E}(\lambda)$ (grey) are calculated using $\mathcal{E}(\lambda) = \det(A_p - I)$ and Eq. (3.21), where $\lambda = \nu + i\omega$. Zeros of the Evans function occur at the crossings of black and grey lines. (a) Lower stable branch at $c = 0.2$; (b) Middle unstable branch at $c = 0.2$; (c) Upper unstable branch at $c = 0.2$, (d) Saddle-node bifurcation at $c = 0.389$. Other parameters are $\kappa = 0.1$, $\alpha = 10$, $\beta = 0.5$, and $I_0 = 0.5$



leaving a single unstable pulse whose linear stability is determined by a positive real eigenvalue. Nonetheless, the spatiotemporal dynamics of the network do evolve to a propagating pulse solution whose width changes periodically, as shown in Fig. 8.

3.4 Bumps

To consider the network dynamics resulting as the rotating input is slowed to a stop, we study the limit of the stimulus speed as $c \rightarrow 0$. In this case, there will be a stationary input, so we will look for stationary solutions, bumps in particular. Such inputs may be applicable to studying the effects of excessive excitation in the network on fixed visual inputs. Therefore, we study the existence and stability of stimulus driven bumps in this section along the lines of previous studies both in a ring model (Ben-Yishai et al. 1995; Bressloff and Cowan 2002) and in an infinite domain (Folias and Bressloff 2004). In this case, the presence of a periodic weight function with inhibition contributes to the possibility of spatially asymmetric instabilities in the bump, as oppose to the reflection symmetric breathers found in Folias and Bressloff (2004, 2005a).

3.4.1 Existence

In the case of a stationary (time-independent) bump solution, the input drive $U(x)$ crosses threshold κ twice. Assuming the stationary input $I(x - ct) \equiv I(x)$ is centered at $x = 0$, threshold crossings will occur at $x = -\Delta, \Delta$ due to the resulting symmetry of the problem. The input drive must be superthreshold when $|x| < \Delta$ and subthreshold otherwise. It is straightforward to show these conditions hold for bumps in the network with linear adaptation, but such stationary bumps do not exist in the network with nonlinear adaptation (Kilpatrick and Bressloff 2010b). The time-

independent version of system (2.1) reduces to the pair of equations

$$U(x) = \int_{-\Delta}^{\Delta} w(x - x')dx' - V(x) + I(x), \tag{3.22}$$

$$V(x) = \beta U(x). \tag{3.23}$$

Substituting (3.23) into (3.22) and using the harmonic weight function yields the solution

$$U(x) = \frac{2}{1 + \beta} [w_0\Delta + w_2 \sin \Delta \cos x] + \frac{I_0}{2(1 + \beta)} (1 + \cos x). \tag{3.24}$$

Note that, using trigonometric identities, we could rewrite the bump solution (3.24) as $U(x) = A \sin(x + B) + C$, so we can be sure the function has a single maximum and minimum, implying it will surely be a single bump. Applying the threshold conditions $U(-\Delta) = U(\Delta) = \kappa$, we arrive at an implicit expression for the bump width

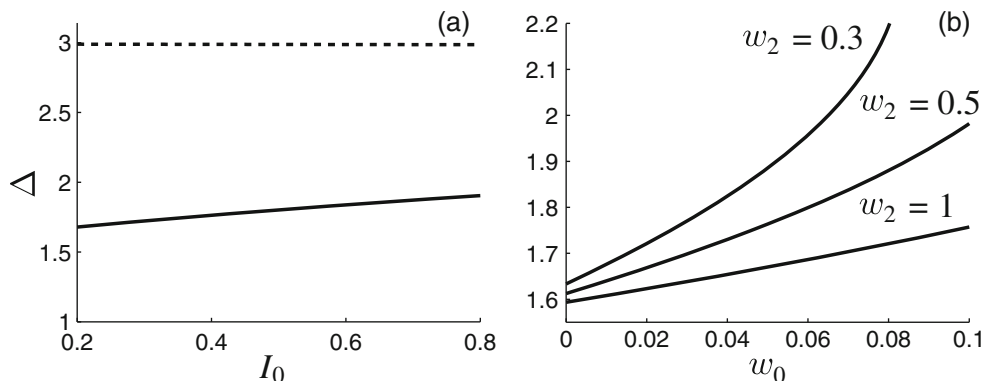
$$\frac{I_0(1 + \cos \Delta) + 4w_0\Delta + 2w_2 \sin(2\Delta)}{2(1 + \beta)} = \kappa. \tag{3.25}$$

We plot the variation of the bump width with the parameters w_0 and I_0 in Fig. 10; the stability of the bump is analyzed below. Notice specifically in Fig. 10b that as the net excitation w_0 is increased, the bump width increases, but the bump width decreases as modulatory strength w_2 increases.

3.4.2 Stability

We can determine the stability of the bump of half-width Δ by writing $u(x, t) = U(x) + e^{\lambda t}\psi(x)$ and $v(x, t) = V(x) + e^{\lambda t}\phi(x)$ with $V(x) = \beta U(x)$ and expanding Eq. (2.1) to first-order in (ψ, ϕ) . Note, we assume small, smooth perturbations of the stationary

Fig. 10 (a) Stable (solid) and unstable (dashed) bump half-widths Δ versus input strength I_0 for $\kappa = 0.1$, $\beta = 0.5$, $w_0 = 0.05$, and $w_2 = 0.5$. (b) Stable bump half-width Δ versus net excitation w_0 for various modulatory strengths w_2 . Here $\kappa = 0.1$, $\beta = 0.5$, and $I_0 = 0.4$



bump solution are separable. Along with the identity (3.19), this leads to the linear equation

$$(\lambda + 1)\psi + \phi = \frac{w(x - \Delta)\psi(\Delta)}{|U'(\Delta)|} + \frac{w(x + \Delta)\psi(-\Delta)}{|U'(-\Delta)|}, \tag{3.26}$$

$$(\alpha\lambda + 1)\phi = \beta\psi, \tag{3.27}$$

where

$$U'(x) = -\frac{(4w_2 \sin \Delta + I_0) \sin x}{2(1 + \beta)}, \tag{3.28}$$

and $U'(-\Delta) = -U'(\Delta) > 0$. Substituting Eq. (3.27) into Eq. (3.26), we obtain the eigenvalue equation

$$\Gamma(\lambda)\psi(x) = (\lambda + \alpha^{-1}) \times \frac{w(x - \Delta)\psi(\Delta) + w(x + \Delta)\psi(-\Delta)}{|U'(\Delta)|}, \tag{3.29}$$

where

$$\Gamma(\lambda) = \lambda^2 + (1 + \alpha^{-1})\lambda + \frac{1 + \beta}{\alpha}.$$

First, considering solutions $\psi(x)$ that vanish at $x = \pm\Delta$ we find $\lambda = \lambda_{\pm}^0$ such that

$$\lambda_{\pm}^0 = \frac{-(1 + \alpha^{-1}) \pm \sqrt{(1 + \alpha^{-1})^2 - 4\alpha^{-1}(1 + \beta)}}{2}.$$

Since λ_{\pm}^0 have infinite multiplicity and always have negative real part, they belong to the essential spectrum and do not contribute to any instabilities. There are then two other solutions to Eq. (3.29). The first are of the form $\psi(x) = A[w(x - \Delta) + w(x + \Delta)]$ with A a constant coefficient and λ given by the roots of the equation

$$\lambda^2 + (1 + \alpha^{-1})\lambda + \alpha^{-1}(1 + \beta) = (\lambda + \alpha^{-1})\frac{w(0) + w(2\Delta)}{|U'(\Delta)|}.$$

This yields the pair of eigenvalues $\lambda = \hat{\lambda}_{\pm}$, where

$$\hat{\lambda}_{\pm} = \frac{-\Lambda_{\pm} \pm \sqrt{\Lambda_{\pm}^2 - 4\alpha^{-1}(1 + \beta)(1 - \Omega_{\pm})}}{2}, \tag{3.30}$$

with

$$\Lambda_{+} = 1 + \alpha^{-1} - (1 + \beta)\Omega_{+},$$

$$\Omega_{+} = \frac{w(0) + w(2\Delta)}{w(0) - w(2\Delta) + \mathcal{I}},$$

and $\mathcal{I} = |U'(\Delta)|$. Finally, there is a solution of the form $\psi(x) = A[w(x - \Delta) - w(x + \Delta)]$ with A a constant coefficient and λ given by the roots of

$$\lambda^2 + (1 + \alpha^{-1})\lambda + \alpha^{-1}(1 + \beta) = (\lambda + \alpha^{-1})\frac{w(0) - w(2\Delta)}{|U'(\Delta)|}.$$

This yields the pair of eigenvalues $\lambda = \lambda_{\pm}$, where

$$\lambda_{\pm} = \frac{-\Lambda_{\pm} \pm \sqrt{\Lambda_{\pm}^2 - 4\alpha^{-1}(1 + \beta)(1 - \Omega_{\pm})}}{2}, \tag{3.31}$$

with

$$\Lambda_{-} = 1 + \alpha^{-1} - (1 + \beta)\Omega_{-},$$

$$\Omega_{-} = \frac{w(0) - w(2\Delta)}{w(0) - w(2\Delta) + \mathcal{I}}.$$

Employing the harmonic weight function (2.6) and noting that $\Delta \in (0, \pi)$, we can make a comparison of the two pairs of eigenvalues easier by evaluating

$$\Omega_{+} = \frac{4(w_0 + w_2 \cos^2 \Delta)}{(I_0 + 4w_2 \sin \Delta) \sin \Delta},$$

$$\Omega_{-} = \frac{4w_2 \sin^2 \Delta}{(I_0 + 4w_2 \sin \Delta) \sin \Delta}.$$

Thus, $\Omega_{-} > \Omega_{+}$ when $\sin^2 \Delta - \cos^2 \Delta > w_0/w_2$ or equivalently when

$$\Delta \in (\Delta_{-}, \Delta_{+}), \quad \Delta_{\pm} = \frac{\pi}{2} \pm \cos^{-1} \left(\frac{w_0}{w_2} \right),$$

otherwise $\Omega_{+} > \Omega_{-}$. This will determine which is the dominant eigenvalue. In Fig. 11, we compute specific eigenvalues for the stimulus driven bumps shown in

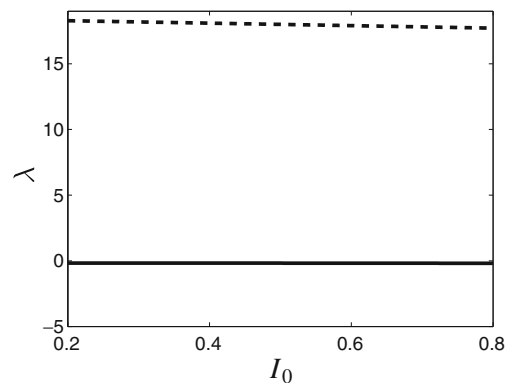


Fig. 11 Maximal eigenvalue associated with the thin (solid) and wide (dashed) bumps pictured in Fig. 10 as a function of I_0 . Other parameters are $\kappa = 0.1, \beta = 0.5, w_0 = 0.05,$ and $w_2 = 0.5$

Fig. 10(a), showing the wide bump is unstable and the thin bump is stable.

4 Nonlinear adaptation

Benda and Herz have derived a reduced firing rate model with an adaptation variable from three different conductance based models with hyperpolarizing currents thought to participate in spike frequency adaptation (Benda and Herz 2003). The adaptation variable has a nonlinear dependence upon the activity variable. Using this idea, a few studies have examined the effects that different forms of nonlinear adaptation have upon spatiotemporal dynamics of firing rate models (Coombes and Owen 2004, 2005; Kilpatrick and Bressloff 2010b). For example, Coombes and Owen (2005) showed that a neural field model with nonlinear adaptation can support breathing bumps and pulses as well as more exotic solutions without any spatially inhomogeneous input being applied (Folias and Bressloff 2004, 2005b). As has been shown in Kilpatrick and Bressloff (2010c), the stability analysis of bumps and traveling pulses in networks with nonlinear adaptation can be much more subtle than in the linear adaptation case due to the piecewise smooth nature of the system’s dynamics. Thus, in our study of the network with nonlinear adaptation we carry out an analysis of the space-clamped system, the existence of the ON state, and existence and stability of traveling pulses. Though, some of these calculations are relegated to the appendix. We show, as a means of comparison to the network with linear adaptation, that most of the expressions are much more straightforward, but some cannot be derived due to the system’s piecewise smoothness. However, in the network with nonlinear adaptation, we cannot study the existence and stability of bumps, since the threshold condition will be violated by the

discontinuity in the adaptation variable (Kilpatrick and Bressloff 2010b).

4.1 Space-clamped system

As with the system with linear adaptation (2.1), we study the space-clamped version of the system with nonlinear adaptation (2.2) in the situation of time-independent and time-periodic input. The system (2.2) then becomes a pair of ordinary differential equations

$$\begin{aligned} \dot{u} &= -u + \bar{w}H(u - v - \kappa) + I(t), \\ \alpha\dot{v} &= -v + \beta H(u - v - \kappa), \end{aligned} \tag{4.1}$$

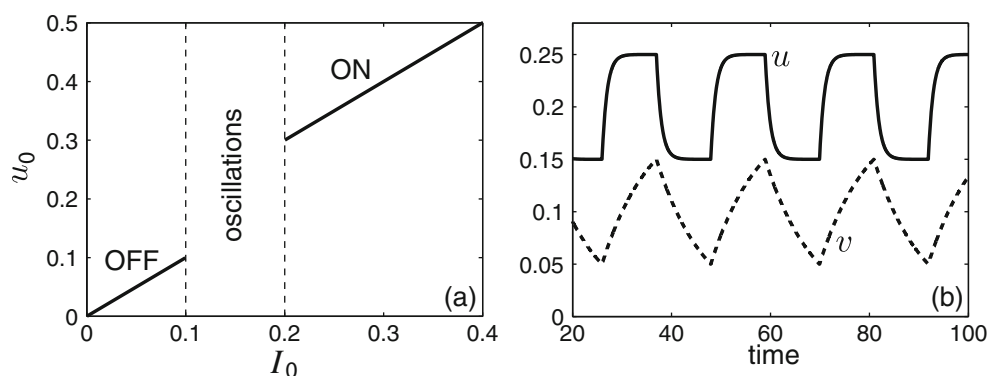
where u and v depend only on t . First, in the limit of infinite rotation speed $c \rightarrow \infty$, the input becomes $I(t) = \bar{I} = \pi I_0$, as in Eq. (3.2). Similarly, the synaptic weight function’s effect can be reduced, in the case of the harmonic weight (2.6), to $\bar{w} = 2\pi w_0$.

To find homogeneous solutions of the full system (2.2), we compute fixed points of the system (4.1) along with their existence conditions

$$\begin{aligned} u_0 = \bar{w} + \bar{I}, \quad v_0 = \beta, \quad &\text{exists if } \bar{w} + \bar{I} > \kappa + \beta, \\ u_0 = \bar{I}, \quad v_0 = 0, \quad &\text{exists if } \bar{I} < \kappa, \end{aligned}$$

and notice a maximum of two fixed points exist, which would both be stable. Thus, the full system (2.2) will support only the ON state if $\bar{I} > \kappa$, only the OFF state if $\bar{w} + \bar{I} < \kappa + \beta$, both ON and OFF states if $\bar{I} < \kappa$ but $\bar{w} + \bar{I} > \kappa + \beta$, and no steady states if $\bar{I} > \kappa$ and $\bar{w} + \bar{I} < \kappa + \beta$. In order for the bistable case to occur, parameters must be restricted as $\beta < \bar{w}$. We illustrate an example of these possibilities in Fig. 12. Also, we show the evolution of the system when there are no steady states and self-sustained oscillations result. It appears the system with nonlinear adaptation is more conducive to oscillations. Low amplitude oscillations like this do not exist in the network with linear adaptation.

Fig. 12 (a) Equilibria of the space-clamped system (4.1) as a function of input I_0 . There is no bistability for this particular choice of parameters since $\beta > \bar{w}$. Other parameters are $\kappa = 0.1$, $\beta = 0.2$. (b) Example of the case with no steady state when $I_0 = 0.15$, so that self-sustained oscillations result



Secondly, we study the effect of a spatially homogeneous, time-periodic input (3.5) with period $2T_I$; this corresponds to a flashing light stimulus. A time-periodic solution may develop, synchronized to the input period $2T_I$. As in the network with linear adaptation, we are interested in finding the critical frequency $\omega^* = 1/2T_I^*$, below which a continuously ON solution does not exist. As before, we do so by solving for the time-periodic, continuously ON solution u to Eq. (4.1) with input (3.5), and identifying where the minimal value of u crosses below κ . This occurs when $u((2T_I)^-) = \kappa$ or

$$\frac{I_0(e^{-T_I} - e^{-2T_I})}{1 - e^{-2T_I}} = \kappa - \bar{w}. \quad (4.2)$$

Notice, this is a much more concise formula than that derived for the network with linear adaptation (3.6). We plot the curves given by Eq. (4.2), partitioning parameter space into flicker and fusion regions in Fig. 13, also showing the effect of increasing net excitation. The network with more excitation can maintain fusion where the network with less does not. These results are qualitatively similar to those found for the network with linear adaptation driven by a flicker stimulus in Fig. 3. However, in the case of nonlinear adaptation, there seems to be a much stronger dependence of the critical flicker half-period T_I^* on input strength I_0 .

4.2 Loss of the ON state

We now examine the critical stimulus speed c_* at which the ON state ceases to exist. This is the speed at which

the network can begin to encode information about the location of the stimulus. Here, we simply present the exact expression for c_* , which we derive in detail in Appendix A

$$c_* = \sqrt{\frac{I_0^2}{(4\pi w_0 + I_0 - 2(\beta + \kappa))^2} - 1}, \quad (4.3)$$

and when $c > c_*$, the ON state exists. Notice, therefore, that when $w_0 < (\beta + \kappa - I_0)/(2\pi)$, the ON state never exists for any value of c , and when $w_0 > (\beta + \kappa)/(2\pi)$, the ON state exists for all values of c . Otherwise, the critical value c_* will indicate the boundary between the ON state and dynamics where $U(\xi) < \beta + \kappa$ for some $\xi \in (-\pi, \pi)$. We plot this boundary in Fig. 14, comparing the effects of different levels of net excitation w_0 . Values of c below the critical curve associated with each value of w_0 do not support the ON state. Notice that the results are qualitatively similar to those derived for the network with linear adaptation. However, one advantage of the result presented here is that it provides an explicit expression for the critical stimulus speed.

4.3 Stimulus-locked pulses

We now present our results regarding stimulus-locked pulses in the network with nonlinear adaptation. Technical issues arise in calculating stability of the traveling pulse here due to the nonlinearity. Coombes and Owen have studied existence and stability of traveling pulses in a network with nonlinear adaptation on an infinite domain (Coombes and Owen 2005). They used different thresholds for the nonlinearity in the activity and adaptation variable equations, allowing them to

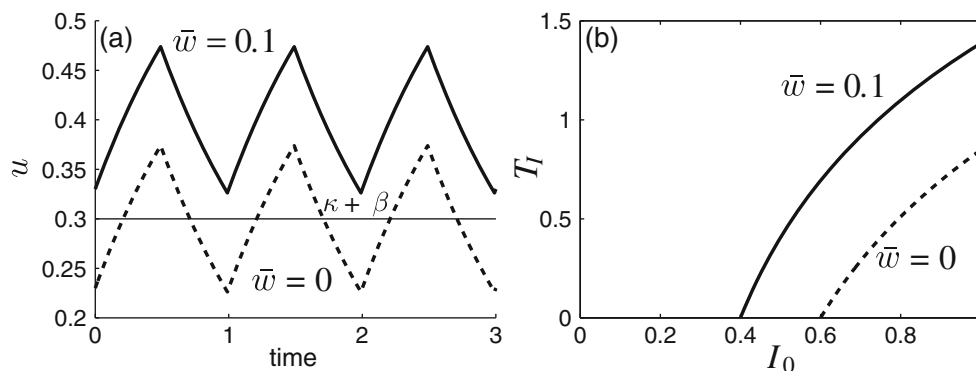
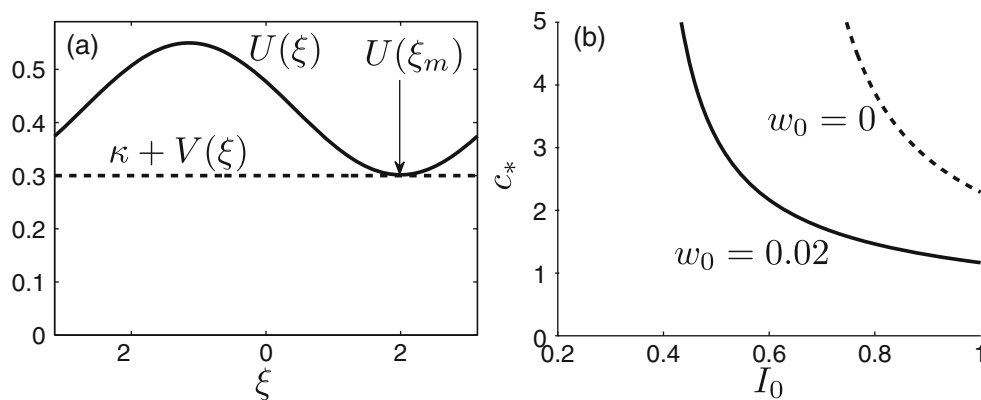


Fig. 13 (a) Evolution of u in time as described by Eq. (4.1) when subject to a flicker stimulus where $T_I = 0.5$ and $I_0 = 0.6$ for low and high net excitation $\bar{w} = 0$. For elevated excitation ($\bar{w} = 0.1$), the input current remains superthreshold ($u > \kappa + \beta$) for the entirety of the stimulus period $2T_I = 1$, while the network with less excitation ($\bar{w} = 0$) does not. (b) Plot of the critical value of T_I

versus input strength I_0 determined by the Eq. (4.2) for low excitation $\bar{w} = 0$ (dashed) and high excitation $\bar{w} = 0.1$ (solid). Above these curves, the input current is not always superthreshold, but represents a flicker of the given period. Below these curves, the input current is always superthreshold, representing a fusion state. Other parameters are $\kappa = 0.1$, $\alpha = 10$, and $\beta = 0.2$

Fig. 14 (a) The ON state plotted for stimulus speed $c = 2.2$ and net excitation $w_0 = 0.02$, slightly above the critical speed for the stimulus strength $I_0 = 0.6$. The minimum $U(\xi_m)$ lies slightly above the total threshold $\kappa + V = 0.3$. (b) Critical value of c_* calculated using Eq. (4.3) plotted versus stimulus strength I_0 for threshold $\kappa = 0.1$. Here $\beta = 0.2$



circumvent issues that might arise in the calculation of the Evans function characterizing stability. As we show in Appendix C, when calculating stability of traveling pulses, we must keep track of the sign of perturbation at the boundaries of the pulse. Recently, this issue was addressed in a study of existence and stability of stationary bumps in a nonlinear model with synaptic depression (Kilpatrick and Bressloff 2010c; Bressloff and Kilpatrick 2011).

4.3.1 Existence

Dependence of traveling pulse solutions on parameters here is qualitatively similar to that found for the network with linear adaptation. Our analysis follows along similar lines too, so our construction of traveling pulse solution lies in Appendix B. Upon constructing the stimulus-locked traveling pulse solutions to the network with nonlinear adaptation (2.2) and Heaviside firing rate function (2.5), we have following nonlinear

system of equations relating their width Δ and shift Δ_I to parameters:

$$w_0\Delta + \frac{I_0}{2} + \frac{I_0[c \sin \Delta_I - \cos \Delta_I]}{2(1 + c^2)} + \frac{w_2[\sin \Delta + c(\cos \Delta - 1)]}{1 + c^2} = \beta \frac{e^{\Delta/\alpha c} - 1}{e^{2\pi/\alpha c} - 1} + \kappa,$$

$$w_0\Delta + \frac{I_0}{2} + \frac{I_0[c \sin(\Delta_I - \Delta) - \cos(\Delta_I - \Delta)]}{2(1 + c^2)} + \frac{w_2[\sin \Delta + c(1 - \cos \Delta)]}{1 + c^2} = \beta \frac{1 - e^{-\Delta/\alpha c}}{1 - e^{-2\pi/\alpha c}} + \kappa,$$

which can be solved numerically. Notice, however, a solution (Δ, Δ_I) is not necessarily a single pulse. This is because there could be additional crossing points of $U - V$ with κ due to the exponential terms in V decaying too steeply. Thus, we must take care in ensuring that

$$U(\xi) - V(\xi) > \kappa : \xi \in (\pi - \Delta, \pi),$$

$$U(\xi) - V(\xi) < \kappa : \xi \in (-\pi, \pi - \Delta). \tag{4.4}$$

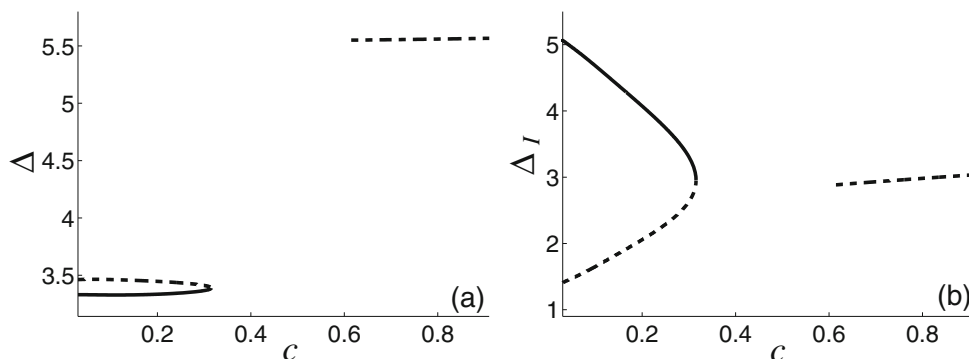
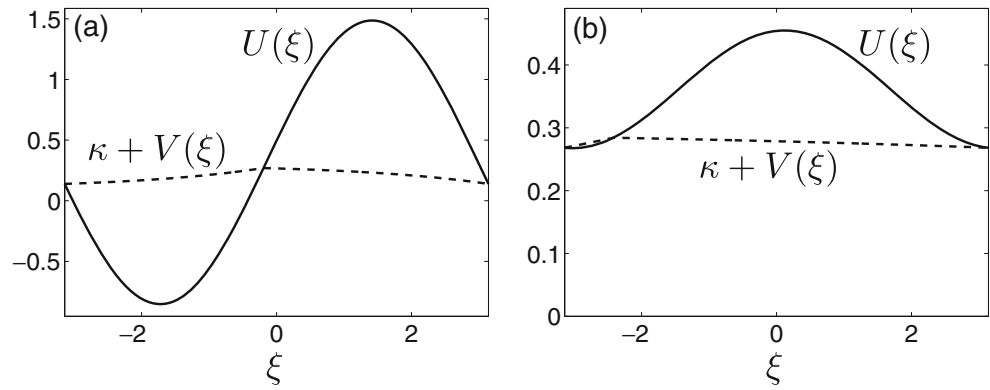


Fig. 15 Dependence of the (a) pulsewidth Δ and (b) input shift Δ_I on the stimulus speed c . There is range of slow speeds for which two traveling pulses solutions exist, one unstable (dashed), one stable (solid). At a critical value of c , two solutions annihilate

one another and a single unstable pulse appears again at higher c values. Other parameters are $\kappa = 0.1, \alpha = 10, \beta = 0.2, w_0 = 0.02, w_2 = 0.5$, and $I_0 = 0.5$

Fig. 16 Profiles of the (a) stable for $c = 0.2$ and (b) unstable pulse for $c = 0.8$. Solutions $U(\xi)$ and $V(\xi)$ given by Eqs. (B.1) and (B.2), respectively. Note that the solution $U(\xi)$ remains above the threshold $V(\xi) + \kappa$ within the region $\xi \in (\pi - \Delta, \pi)$. Other parameters are $\kappa = 0.1, \alpha = 10, \beta = 0.2, w_0 = 0.02, w_2 = 0.05,$ and $I_0 = 0.5$



Such issues do not arise in the network with linear adaptation because the auxiliary variable does not directly affect the subthreshold or superthreshold conditions of the traveling pulses.

The dependence of pulse width Δ and input shift Δ_I on various parameters is shown in Fig. 15, and example profiles of a stable and unstable pulse in Fig. 16. Notice the rise and fall of the input U and adaptation V variables is much more synched than in the case of linear adaptation. As $c \rightarrow 0$, there is a range of stimulus speeds for which no stimulus-locked pulses exist, since the solutions we construct violate the subthreshold and superthreshold assumptions (4.4). We find propagating and nonpropagating breathers can result in this slow c parameter range. Beyond this range, solutions and stability are qualitatively similar to the linear adaptation case, and we associate the onset of trailing phenomena with the critical value of c where the saddle-node bifurcation exists. Parameter space is partitioned into existing stable solutions in Fig. 17 for both (w_2, c) and

(I_0, c) . Numerical simulations of different scenarios of stimulus-locked pulses are pictured in Fig. 18.

4.3.2 Stability

We now show stability results for stimulus-driven pulses in the network with nonlinear adaptation. In the study of a similar network by Coombes and Owen, it was shown that in the case of no external stimuli, a network with nonlinear adaptation can support pulses that lose stability through a supercritical Hopf bifurcation (Coombes and Owen 2005). Their stability calculation was eased by the fact that they took different threshold values for the nonlinearities in the adaptation versus activity variable. Hopf instabilities in traveling pulses result in traveling breathers. The stability calculation for traveling pulses in the network with nonlinear adaptation (2.2) requires more care due to there being a jump discontinuity in the derivative $V'(\xi)$ at the threshold crossing points $\xi = \pi - \Delta$ and π .

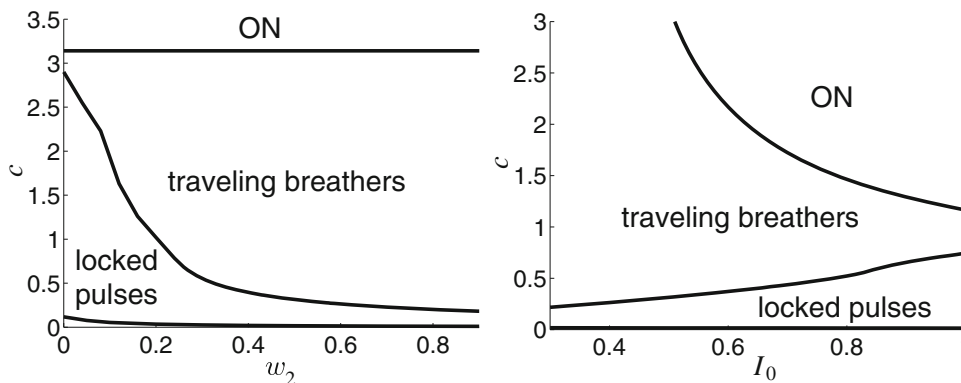


Fig. 17 (a) Partition of (w_2, c) parameter space, where $I_0 = 0.5$, into three different behaviors of solutions. For sufficiently slow stimuli, the network can track the signal as a translationally invariant traveling pulse. As the stimulus speed increases, there is a critical value of c at which stable pulses cease to exist and the invariant solution slips off of the stimulus, leading to traveling

breathers. This corresponds to discrete afterimages at each slip time. For very fast stimuli, the ON state exists, corresponding to the whole domain being superthreshold. (b) Similar partition of (I_0, c) parameter space for $w_2 = 0.5$. Other parameters are $\kappa = 0.1, \alpha = 10, \beta = 0.2,$ and $w_0 = 0.02$

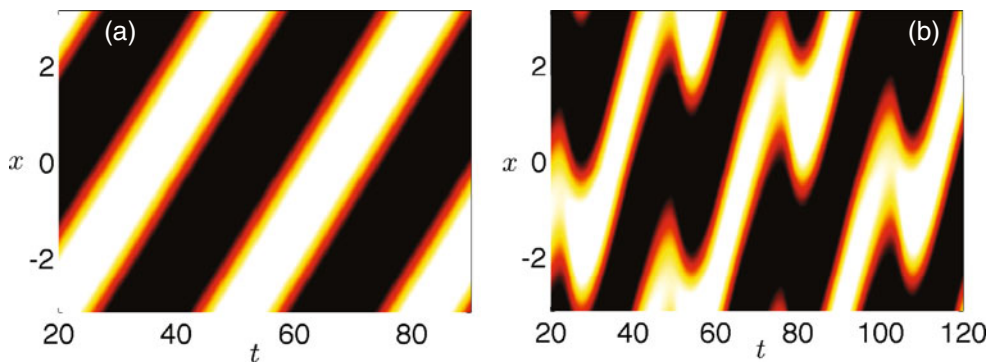


Fig. 18 Numerical simulations of stimulus-locked pulses and traveling breathers in the network with nonlinear adaptation (2.2) for a Heaviside firing rate (2.5), where $u(x, t) - v(x, t)$ is plotted. (a) For a speed ($c = 0.2$) within the region of parameter space where stable locked traveling pulses exist. (b) For a speed

($c = 0.4$) beyond the critical speed where stable pulses cease to exist, superthreshold activity periodically lurches, representative of a discrete afterimage. Other parameters are $\kappa = 0.1$, $\alpha = 10$, $\beta = 0.2$, $w_0 = 0.02$, $w_2 = 0.5$, and $I_0 = 0.5$

We demonstrate the detailed calculation of the Evans function, whose zeros are associated with the linear stability of stimulus-locked pulses, in Appendix C. The resulting spectral equation then depends on the sign of the perturbation at these crossing points, which in turn determines associated eigensolutions.

We can use our Evans function calculation to compute real eigenvalues for the traveling pulse solutions of Fig. 18. As opposed to the case of the network with linear adaptation, we find the zeros of the Evans function by plotting the zero contours of $\mathcal{E}(\lambda) = \det(\mathcal{A}_p - I)$ in (c, λ) space assuming λ is real. This requires finding the real eigenvalues of \mathcal{A}_p defined by Eq. (C.10) for four different restricted classes of eigenvectors, defined in

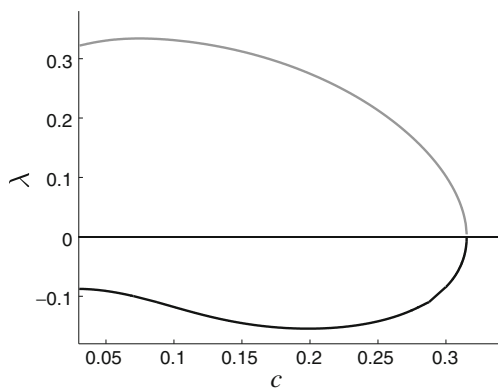


Fig. 19 Maximal eigenvalues associated with linear stability of stimulus-driven pulses (B.1) and (B.2), whose width Δ and shift Δ_I are plotted in Fig. 15. These are computed as the real zeros of the Evans function $\mathcal{E}(\lambda) = \det(\mathcal{A}_p - I)$ with Eq. (C.10). The upper branch of pulses in Fig. 15 will be unstable, as determined by positive eigenvalues (grey), and the lower branch of pulses will likely be stable, since eigenvalues are negative (black). Parameters are $\kappa = 0.1$, $\alpha = 10$, $\beta = 0.2$, $w_0 = 0.02$, $w_2 = 0.5$, and $I_0 = 0.5$

Appendix C. In Fig. 19, we plot the maximal real eigenvalue associated with the stability of each traveling pulse solution in Fig. 18 for $c \in (0.02, 0.32)$. Specifically, we find that the wide pulse is always unstable and the narrower pulse is always stable, as long as they exist. Both eigenvalues approach zero as the pulse widths approach one another. We also found that the maximal real eigenvalue associated with the single pulse solution at larger c values is always positive (not shown).

5 Continuous firing rate functions and larger domains

We now study extensions of the full systems (2.1) and (2.2) beyond the case of a Heaviside firing rate function (2.5) with a 2π -periodic domain. In particular, we are interested in the effects of using continuous firing rate function like the sigmoid (2.3) and piecewise linear (2.4) as well as the effect of expanding size of periodic domain we are examining. The benefit of our previous assumptions on the firing rate function, weight function, and input were that they allowed us to develop analytic expressions for boundaries in parameter space separating different spatiotemporal dynamics of the networks. Especially in the case of the network with nonlinear adaptation (2.2), these analytical expressions are straightforward to examine and allow an understanding of the role each parameter plays in determining network behavior. We cannot derive such expressions for the examples in this section. Thus, we resort to numerical simulations of the network to see how our predictions of our analysis from Sections 3 and 4 extend to these examples.

Using the same parameter values as our examples in Section 3, for the network with linear adaptation (2.1),

we find qualitatively similar results for the relationship between stimulus speed and the form of the resulting solution. In Fig. 20, we show two example simulations similar to that pictured in Fig. 8(b) for the Heaviside firing rate. The behavior of the model with a sigmoid firing rate, even for a fairly low gain of $\eta = 10$, is quite similar to that with infinite gain. We found through numerical simulations that the switch from locked pulses to traveling breathers occurs at a stimulus speed of roughly $c = 0.4$, which is not too far removed from that predicted in the system with the Heaviside firing rate (2.5). Likewise, we found the onset of traveling breathers beyond a critical stimulus speed of roughly $c = 0.5$ for the network with a piecewise linear firing rate with slope $\gamma = 2$. For weak inputs (not shown), firing rate functions do not saturate but networks with continuous firing rate functions exhibit the same transitions between locked and breathing pulses and the speed at which the transition between these two behaviors decreases as synaptic modulation increases. When inputs become sufficiently weak, there is no transition to the ON state as c is increased to infinity, just as we found for networks with Heaviside firing rate.

We carried out such simulations for other parameter sets as well for both networks, with linear and nonlinear adaptation (not shown). Overall, it appears using a sigmoid with finite gain or a piecewise linear function does not drastically alter the dynamics existent in the system. Therefore we conclude that using the Heaviside firing rate for the bulk of our theoretical predictions in this paper is a reasonable approximation. In general, the firing rate of a neuron or population of neurons is known to be a continuous function input current. Therefore, the validity of our predictions in previous sections relies on the reduction of the firing rate to

a piecewise constant function being a justifiable first order approximation.

Now, we turn to studying the networks with both a sigmoidal firing rate function (2.3) as well as the alternative weight function (2.7) in a larger periodic domain, specifically $L = 10\pi$. In addition we use a Gaussian input stimulus (2.9) to the network. In general, we find similar results to those of the smaller network with $L = \pi$ for the transitions of stimulus-locked traveling pulses. Network activity locks to the input stimulus, when it moves below a certain critical speed and there is sufficient inhibition in the network. In both networks with linear and nonlinear adaptation, the pulse begins to breathe beyond a critical stimulus speed. This transition can also occur if inhibition strength is lowered, raising the net excitation of the network.

Numerical simulation results are shown for the network with linear adaptation in Fig. 21. Results are qualitatively similar for the network with nonlinear adaptation, so that the transition to breathing can occur by either increasing input speed c or decreasing inhibition strength A_i . For faster input speeds, the oscillations in the size of the traveling pulse become drastic enough such that there is a period of no superthreshold activity. This would correspond to the input being temporarily invisible. Such a representation of a moving image is commensurate with personal reports of visual trails arising in HPPD. The percept has been compared to a multiple exposure stroboscopic photograph (Dubois and VanRullen 2011). Also, for sufficiently large domain size L , we found the ON state did not exist for realistic input strengths I_0 , no matter how large the speed of the input stimulus. Note, we could approximate very large domains as being infinite and proceed to analyze the networks (2.1) and (2.2) along the lines of previous

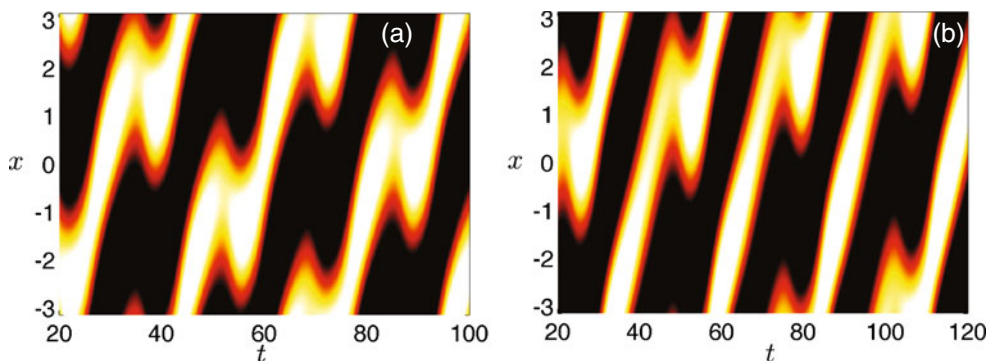


Fig. 20 Numerical simulations of traveling breathers in the network with linear adaptation (2.1) for (a) sigmoidal firing rate (2.3) with gain $\eta = 10$ and (b) piecewise linear firing rate with slope $\gamma = 2$, where $u(x, t)$ is plotted. Both networks receive input

with speed $c = 0.6$ so that superthreshold activity periodically lurches, representative of a discrete afterimage. Other parameters are $\kappa = 0.1$, $\alpha = 10$, $\beta = 0.5$, $w_0 = 0.02$, $w_2 = 0.5$, and $I_0 = 0.5$

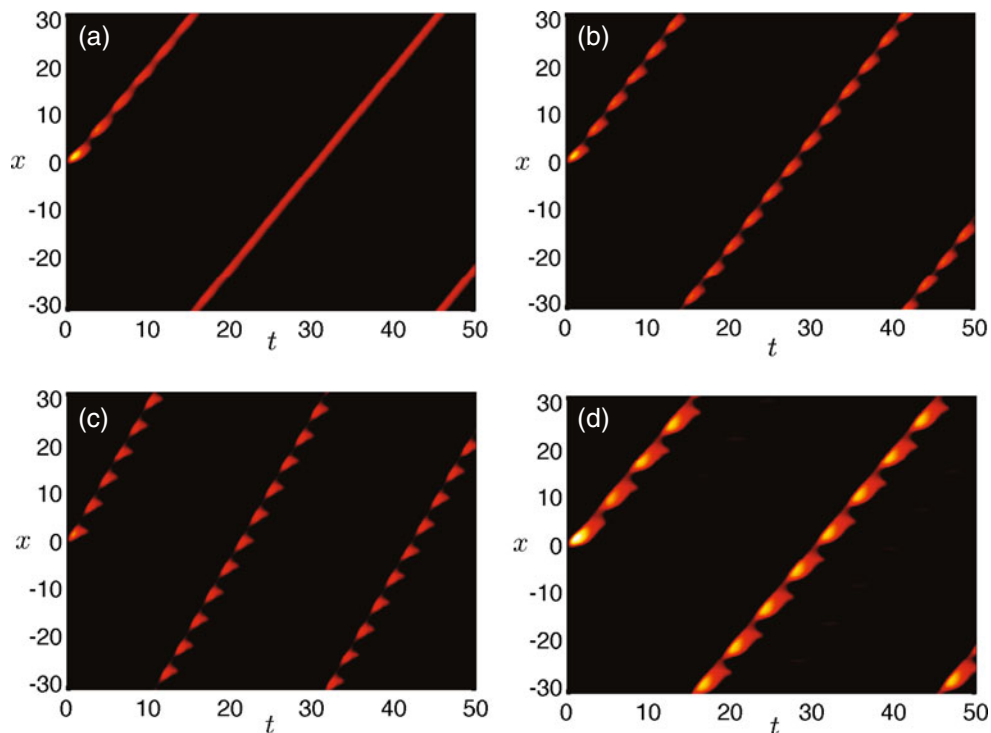


Fig. 21 Numerical simulations of stimulus-locked and breathing pulses in the network with linear adaptation (2.1) for a larger domain where $L = 10\pi$, where $u(x, t)$ is plotted. Firing rate is sigmoidal with gain $\eta = 50$ and threshold $\kappa = 0.1$. Weight function is difference of exponentials (2.7) with spatial scales $\sigma_e = 1$ and $\sigma_i = 2$. Input is Gaussian with strength $I_0 = 0.6$ and spatial scale $\sigma_I = 1$. (a) For $A_i = 0.7$ and $c = 2.1$, stable locked traveling

pulses exist. (b) For $A_i = 0.7$ and $c = 2.3$, pulses lose stability to lurchers. (c) For $A_i = 0.7$ and $c = 3$, superthreshold activity flickers on and off. (d) For $A_i = 0.6$ (more net excitation), traveling pulses can lose stability at the lower stimulus speed $c = 2.1$, compare with stable pulses in (a). Other parameters are $\alpha = 10$ and $\beta = 1$

studies such as Folias and Bressloff (2005b), Coombes and Owen (2005) and Ermentrout et al. (2010). Indeed, we find our numerical simulations of the larger network reveal some of the behaviors studied in Folias and Bressloff (2005b).

6 Discussion

In this paper, we have analyzed the spatiotemporal dynamics induced by time-dependent stimuli in two neuronal networks with adaptation. For spatially homogeneous time-periodic inputs, we could calculate the critical input frequency below which the network resolves the signal, motivated by experimental studies of HPPD patients' ability to track the frequency of a flickering light (Abraham and Wolf 1988). The expression relating parameters to the critical frequency is simpler and explicit for the network with nonlinear adaptation. For translationally invariant moving stimuli, we find a transition between an ON state and a pulse occurred when the stimulus speed is reduced

below a critical value. Both models support stimulus-locked pulses for sufficiently slow stimuli and traveling breathers for intermediate speeds over a wide range of parameters. However, the linear stability calculations for stimulus-locked pulses are particularly more involved for the model with nonlinear adaptation. As the strength of modulation of synaptic connections is increased, we find that the range of traveling breathers increases. In the context of our model, we consider traveling breathers to represent the phenomena of visual trails experienced during HPPD.

Our study adds to the existing theoretical framework for stimulus-induced activity patterns in neural field models with negative feedback. Ben Yishai and colleagues have examined network dynamics induced by weak inputs in a network with excitatory and inhibitory populations with piecewise linear firing rate function (Ben-Yishai et al. 1997). For stationary stimuli, increased modulation of synapses led to a sharpening of input representation. They found that network activity locked to moving stimuli for slow enough stimulus speeds, and the critical speed was related

to the speed of intrinsically generated waves in the network. In a related study, Hansel and Sompolinsky found stationary inputs could pin activity around the input location in a network with adaptation (Hansel and Sompolinsky 1998). However, they did not pursue the effects of moving inputs on adaptive networks. We build on these studies by examining strong inputs in a network with adaptation, rather than inhibition, as its auxiliary variable. Our analysis allows an exact prediction of the boundary of stimulus locking. While increased strength of synaptic modulation can sharpen the response to stationary stimuli, it lowers the critical speed beyond which the network locks to moving stimuli. Thus, synaptic modulation by LSD may last for an extended period of time (Nichols and Sanders-Bush 2002), leading to the shorter time scale dynamics of breathing pulses brought about by the interplay of synaptic signaling and adaptation. We also note that the general behavior of our models is largely independent of the type of firing rate function used. For the sigmoid, piecewise linear, and Heaviside function, increasing the strength of synaptic modulation still widens the range of stimulus speeds that lead to traveling breathers.

Folias and Bressloff studied stimulus-locked traveling pulses in a purely excitatory network with linear adaptation, finding pulses can destabilize through a supercritical Hopf bifurcation when stimulus amplitude is weak enough (Folias and Bressloff 2005b). Traveling breathers in their network either expand and contract or emit secondary pulses due to the purely excitatory and nonperiodic synaptic connectivity. In contrast, the traveling breathers in our study exclusively lose stability through a shift instability. The initial movement of the network dynamics as it loses track of the solution is to slip backwards off of the stimulus. It appears that this requires nonlocal inhibition, considering it is shown in Ben-Yishai et al. (1997) too. Also in contrast to Folias and Bressloff (2005b), the bifurcation structure of pulses in our model, shown by Fig. 5, indicates that traveling breathers arise beyond a saddle-node bifurcation. These unstable oscillating pulses exist subcritically, as suggested by the high amplitude oscillations in the pulsewidth at the onset. Our work does share the similarity with Folias and Bressloff (2005b) in that both employ adaptation as the dynamic negative feedback in the model. The timescale of breathing oscillations in the larger domain system, pictured in Fig. 21, is therefore set by the adaptation timescale, as in Folias and Bressloff (2005b). Stroboscopic visual trailing imagery moves at perceivable timescales of hundreds of milliseconds (Abraham 1983; Dubois and VanRullen 2011), making adaptation a more likely candidate mechanism than fast inhibitory synapses.

By considering this work in the context of neural activity in V1 induced by visual inputs, we can relate our results to extensive experimental findings related to HPPD. Traveling breathers, particularly ones that slip backwards, are representative of the experience of discrete afterimages seen by HPPD sufferers that trail behind a moving visual input (Horowitz 1969; Abraham 1983; Halpern and Pope 2003). We propose that, for the period of time that an afterimage is seen, there is a population of neurons in V1 that is superthreshold, despite their receiving no input stimulus at that time. In our networks, simply increasing net excitation w_0 leads to wider representation of input stimuli, suggestive of the halos seen in HPPD (Abraham 1983). However, the strength of synaptic modulation w_2 is the main parameter in our models responsible for altering how well the network can represent moving stimuli. Maintaining the balance of excitation and inhibition while increasing the strength of each leads to less faithful representations. This theory matches well with that findings that LSD can boost glutamatergic receptor expression (Nichols and Sanders-Bush 2002), and drugs that induce similar trailing phenomena to HPPD can increase serotonin levels (Boyer and Shannon 2005; Fontenelle 2008). Taken with the fact that timescales of the model dynamics are commensurate with stroboscopic imagery, our model appears to explain several characteristics of HPPD phenomena.

In future work, it would be interesting to study other types of solutions that could arise in stimulus-driven neuronal networks with adaptation. In particular, Troy and Shusterman have shown that traveling multi-pulses can arise in a neuronal network with linear adaptation and no stimuli (Troy and Shusterman 2007). Studying the existence and stability traveling multi-pulses in stimulus-driven networks may shed light on proper and pathological visual processing as they relate to physiological parameters. In addition, Coombes and Owen showed that exotic solutions like self-replicating bumps can arise in neuronal networks with nonlinear adaptation for fairly strong adaptation (Coombes and Owen 2005). These types of solutions have not been observed in the case of linear adaptation. It would be interesting to examine how spike frequency adaptation aids or hinders the proper processing of a variety of inputs, particularly how this depends on the form of adaptation included in a firing rate model.

Acknowledgements We would like to thank Julien Dubois for sharing with us reports from subjects regarding the specifics of visual trails due to HPPD. We also thank Henry Abraham for use of his patient's drawing of a visual trails experience. ZPK is supported by an NSF Mathematical Sciences Postdoctoral

Research Fellowship (DMS-1004422). GBE is supported by an NSF grant (DMS-0817131).

Appendix A: ON state in system with nonlinear adaptation

In this appendix, we derive Eq. (4.3), giving the critical speed c_* at which the ON state ceases to exist in the full network with nonlinear adaptation (2.2). Thus, we study the equations,

$$\begin{aligned}
 u_t &= -u + \int_{-\pi}^{\pi} (w_0 + w_2 \cos(x - x')) \\
 &\quad \times H(u(x', t) - v(x', t) - \kappa) dx' + I_0 \cos^2\left(\frac{x - ct}{2}\right), \\
 v_t &= (-v + \beta H(u - v - \kappa)) / \alpha.
 \end{aligned}
 \tag{A.1}$$

Changing coordinates to the rotating frame $\xi = x - ct$, so $u = U(\xi)$ and $v = V(\xi)$, and assuming the ON state exists ($U(\xi) > V(\xi) + \kappa$), we have

$$\begin{aligned}
 -cU'(\xi) &= -U(\xi) + \int_{-\pi}^{\pi} w_0 + w_2 \cos(\xi - \xi') d\xi' \\
 &\quad + I_0 \cos^2\left(\frac{\xi}{2}\right), \\
 -cV'(\xi) &= (-V(\xi) + \beta) / \alpha.
 \end{aligned}$$

Solving this pair of first order differential equations by along with periodic boundary conditions yields

$$U(\xi) = 2\pi w_0 + \frac{I_0}{2} + \frac{I_0(\cos \xi - c \sin \xi)}{2(1 + c^2)}
 \tag{A.2}$$

and $V(\xi) = \beta$. For the ON state to exist, synaptic input must be superthreshold, $U(\xi) > \kappa + \beta$ for all $\xi \in (-\pi, \pi)$. Simply requiring this of the minimum, $U(\xi_m) > \kappa + \beta$, yields the following inequality

$$2\pi w_0 + \frac{I_0(\sqrt{1 + c^2} - 1)}{2\sqrt{1 + c^2}} > \beta + \kappa.
 \tag{A.3}$$

We then identify the critical stimulus speed value c_* at which the ON state ceases to exist as that for which the inequality (A.3) becomes a strict equality. Thus, we can solve the equality explicitly for Eq. (4.3):

$$c_* = \sqrt{\frac{I_0^2}{(4\pi w_0 + I_0 - 2(\beta + \kappa))^2}} - 1,$$

so when $c > c_*$, the ON state exists.

Appendix B: Existence of pulses in network with nonlinear adaptation

Here, we present our construction of stimulus-locked traveling pulse solutions in the network with nonlinear adaptation (2.2) and Heaviside firing rate function (2.5). Changing to traveling wave coordinates $\xi = x - ct$, a pulse of width $\Delta \in (0, 2\pi)$ has superthreshold region $\xi \in (\pi - \Delta, \pi)$, where we can arbitrarily select the leading edge’s location due the translation invariance of the problem. We also specify a spatial shift Δ_I of the input $I(x, t) = I_0 \cos^2((\xi + \Delta_I)/2)$. This yields

$$\begin{aligned}
 -cU'(\xi) &= -U(\xi) + \int_{\pi - \Delta}^{\pi} w(\xi - \xi') d\xi' \\
 &\quad + I_0 \cos^2\left(\frac{\xi + \Delta_I}{2}\right), \\
 -cV'(\xi) &= (-V(\xi) + \beta \Theta(\xi)) / \alpha,
 \end{aligned}$$

where

$$\Theta(\xi) = \begin{cases} 1, & \xi \in (\pi - \Delta, \pi), \\ 0, & \xi \in (-\pi, \pi - \Delta). \end{cases}$$

Solving this set of equations with periodic boundary conditions gives

$$\begin{aligned}
 U(\xi) &= w_0 \Delta + \frac{I_0[\cos(\xi + \Delta_I) - c \sin(\xi + \Delta_I)]}{2(1 + c^2)} \\
 &\quad + \frac{I_0}{2} + \frac{w_2(\sin \xi - \sin(\xi + \Delta))}{1 + c^2} \\
 &\quad + \frac{w_2 c(\cos \xi - \cos(\xi + \Delta))}{1 + c^2},
 \end{aligned}
 \tag{B.1}$$

$$\begin{aligned}
 V(\xi) &= \beta \left(1 - \frac{e^{\xi/\alpha c} - e^{(\xi + \Delta - 2\pi)/\alpha c}}{2 \sinh(\pi/\alpha c)} \right) : \xi \in (\pi - \Delta, \pi), \\
 V(\xi) &= \beta \left(\frac{e^{(\xi + \Delta)/\alpha c} - e^{\xi/\alpha c}}{2 \sinh(\pi/\alpha c)} \right) : \xi \in (-\pi, \pi - \Delta).
 \end{aligned}
 \tag{B.2}$$

Therefore, to specify the pulse width Δ and associated shift to the input Δ_I , we impose self consistency by requiring that the input current $U(\xi) - V(\xi)$ specified by Eqs. (B.1) and (B.2) cross firing threshold κ at the leading and trailing edge of the pulse such that $U(\pi) - V(\pi) = U(\pi - \Delta) - V(\pi - \Delta) = \kappa$. This generates the following nonlinear system of equations

$$\begin{aligned}
 w_0 \Delta + \frac{I_0}{2} + \frac{I_0[c \sin \Delta_I - \cos \Delta_I]}{2(1 + c^2)} \\
 + \frac{w_2[\sin \Delta + c(\cos \Delta - 1)]}{1 + c^2} = \beta \frac{e^{\Delta/\alpha c} - 1}{e^{2\pi/\alpha c} - 1} + \kappa,
 \end{aligned}$$

$$w_0\Delta + \frac{I_0}{2} + \frac{I_0[c \sin(\Delta_I - \Delta) - \cos(\Delta_I - \Delta)]}{2(1 + c^2)} + \frac{w_2[\sin \Delta + c(1 - \cos \Delta)]}{1 + c^2} = \beta \frac{1 - e^{-\Delta/\alpha c}}{1 - e^{-2\pi/\alpha c}} + \kappa.$$

Appendix C: Stability of pulses in network with nonlinear adaptation

In this appendix, we derive the linear stability approximation for traveling pulses in the network with nonlinear adaptation. As in the case of the network with linear adaptation, we start by considering the evolution of small, smooth perturbations to the traveling pulse solution $(U(\xi), V(\xi))$, such that $u(\xi, t) = U(\xi) + \bar{\psi}(\xi, t)$ and $v(\xi, t) = V(\xi) + \bar{\phi}(\xi, t)$. Upon plugging these expression into the system (2.2) and expanding to first order in $(\bar{\psi}, \bar{\phi})$, we arrive at the system of linear equations

$$\begin{aligned} \bar{\psi}_t - c\bar{\psi}_\xi + \bar{\psi} &= \int_{-\pi}^{\pi} w(\xi - \xi') H'(U(\xi') - V(\xi') - \kappa) \\ &\quad \times (\bar{\psi}(\xi', t) - \bar{\phi}(\xi', t)) d\xi', \\ \bar{\phi}_t - c\bar{\phi}_\xi + \frac{\bar{\phi}}{\alpha} &= \frac{\beta}{\alpha} H'(U - V - \kappa) (\bar{\psi} - \bar{\phi}). \end{aligned}$$

To characterize some of the spectrum of this operator, we can look, in particular, for solutions of the form $(\bar{\psi}, \bar{\phi}) = e^{\lambda t}(\psi(\xi), \phi(\xi))$ and using the identity

$$\frac{dH(U - V - \kappa)}{dU} = \frac{\delta(\xi - \pi + \Delta)}{|U'(\pi - \Delta) - V'(\pi - \Delta)|} + \frac{\delta(\xi - \pi)}{|U'(\pi) - V'(\pi)|}, \tag{C.1}$$

where

$$\begin{aligned} U'(\pi) &= \frac{w_2[\cos \Delta - 1 - c \sin \Delta]}{1 + c^2} + \frac{I_0[\sin \Delta_I + c \cos \Delta_I]}{2(1 + c^2)}, \\ U'(\pi - \Delta) &= \frac{w_2[1 - \cos \Delta - c \sin \Delta]}{1 + c^2} + \frac{I_0[\sin(\Delta_I - \Delta) + c \cos(\Delta_I - \Delta)]}{2(1 + c^2)}. \end{aligned}$$

Due to the jump discontinuity in $V'(\xi)$ at the threshold crossing points, either $V'(\pi) = V'_+(\pi)$ or $V'(\pi) =$

$V'_-(\pi)$, and similarly either $V'(\pi - \Delta) = V'_+(\pi - \Delta)$ or $V'(\pi - \Delta) = V'_-(\pi - \Delta)$ where

$$V'_+(\pi) = -\frac{\beta(1 - e^{(\Delta - 2\pi)/\alpha c})}{\alpha c(1 - e^{-2\pi/\alpha c})}, \tag{C.2}$$

$$V'_-(\pi) = \frac{\beta(e^{\Delta/\alpha c} - 1)}{\alpha c(e^{2\pi/\alpha c} - 1)}, \tag{C.3}$$

$$V'_+(\pi - \Delta) = -\frac{\beta(e^{-\Delta/\alpha c} - e^{-2\pi/\alpha c})}{\alpha c(1 - e^{-2\pi/\alpha c})}, \tag{C.4}$$

$$V'_-(\pi - \Delta) = \frac{\beta(1 - e^{-\Delta/\alpha c})}{\alpha c(1 - e^{-2\pi/\alpha c})}. \tag{C.5}$$

Note that, following recent studies of the stability of spatially structured solutions in piecewise smooth neural fields (Kilpatrick and Bressloff 2010a, c; Bressloff and Kilpatrick 2011), the particular choice to make for each $V'(\pi)$ and $V'(\pi - \Delta)$ will be assigned based the sign of the difference of perturbations $(\psi(\xi) - \phi(\xi))$ in both places the expression appears in the identity (C.1). This is due to the piecewise smooth nature of V' at the boundary of the pulse. Upon assuming a fixed sign of these perturbations, we can only calculate real eigenvalues associated with the resulting piecewise defined system. This is due to the fact that solutions $\psi(\xi) - \phi(\xi)$ with associated complex eigenvalues will oscillate above and below zero, violating our assumption of a fixed sign. Thus, we obtain the following system

$$\begin{aligned} -c\psi' + (\lambda + 1)\psi &= \chi_\pi w(\xi - \pi)(\psi(\pi) - \phi(\pi)) \\ &\quad + \chi_{\pi - \Delta} w(\xi - \pi + \Delta) \\ &\quad \times (\psi(\pi - \Delta) - \phi(\pi - \Delta)) \\ -c\phi' + (\lambda + \alpha^{-1})\phi &= \frac{\beta}{\alpha} [\chi_\pi \delta(\xi - \pi)(\psi(\pi) - \phi(\pi)) \\ &\quad + \chi_{\pi - \Delta} \delta(\xi - \pi + \Delta) \\ &\quad \times (\psi(\pi - \Delta) - \phi(\pi - \Delta))], \end{aligned} \tag{C.6}$$

where

$$\chi_\xi^{-1} = \begin{cases} |U'(\xi) - V'_+(\xi)|, & \text{if } \psi(\xi) < \phi(\xi), \\ |U'(\xi) - V'_-(\xi)|, & \text{if } \psi(\xi) > \phi(\xi). \end{cases} \tag{C.7}$$

Therefore, the stability of the stimulus-locked traveling pulse given by Eqs. (B.1) and (B.2) can be calculated using spectrum of the eigenvalue problem (C.6). First, note that the values bounding the essential spectrum $\lambda = -1$ and $\lambda = -\alpha^{-1}$ have infinite multiplicity and will not contribute to any instabilities. Upon omitting these value from our analysis, we can proceed by solving for the eigenfunctions. It is straightforward to do so by directly integrating both equations, treating the

$\psi(\pi), \psi(\pi - \Delta), \phi(\pi), \phi(\pi - \Delta)$ terms as constants, to find

$$\begin{aligned} \psi(\xi) = & \chi_\pi \left[\mathcal{P}_0 + \frac{\mathcal{P}_1 \sin \xi - \mathcal{P}_2 \cos \xi}{\mathcal{D}_p} \right] (\psi(\pi) - \phi(\pi)) \\ & + \chi_{\pi-\Delta} \left[\mathcal{P}_0 + \frac{\mathcal{P}_1 \sin(\xi + \Delta) - \mathcal{P}_2 \cos(\xi + \Delta)}{\mathcal{D}_p} \right] \\ & \times (\psi(\pi - \Delta) - \phi(\pi - \Delta)), \end{aligned} \tag{C.8}$$

$$\begin{aligned} \phi(\xi) = & \frac{\beta}{\alpha c} \left\{ \chi_\pi \left[\frac{1}{\mathcal{P}_3} - H(\xi - \pi) \right] (\psi(\pi) - \phi(\pi)) \right. \\ & + \chi_{\pi-\Delta} \left[\frac{1}{\mathcal{P}_3} - H(\xi - \pi + \Delta) \right] e^{\frac{\alpha\lambda+1}{\alpha c} \Delta} \\ & \left. \times (\psi(\pi - \Delta) - \phi(\pi - \Delta)) \right\} e^{\frac{\alpha\lambda+1}{\alpha c} (\xi-\pi)}, \end{aligned} \tag{C.9}$$

where

$$\begin{aligned} \mathcal{P}_0 &= \frac{w_0}{\lambda + 1}, \\ \mathcal{P}_1 &= w_2 c, \\ \mathcal{P}_2 &= w_2 (\lambda + 1), \\ \mathcal{P}_3 &= 1 - e^{-\frac{2(\alpha\lambda+1)\pi}{\alpha c}}, \\ \mathcal{D}_p &= (\lambda + 1)^2 + c^2. \end{aligned}$$

Requiring self-consistency of the the solutions (C.8) and (C.9), we generate the following 2×2 system of equations $\psi - \phi = \mathcal{A}_p(\psi - \phi)$ where

$$\begin{aligned} \psi &= \begin{pmatrix} \psi(\pi) \\ \psi(\pi - \Delta) \end{pmatrix}, \quad \phi = \begin{pmatrix} \phi(\pi) \\ \phi(\pi - \Delta) \end{pmatrix}, \\ \mathcal{A}_p &= \begin{pmatrix} \mathcal{A}_{\pi\pi} & \mathcal{A}_{\pi\Delta} \\ \mathcal{A}_{\Delta\pi} & \mathcal{A}_{\Delta\Delta} \end{pmatrix}, \end{aligned} \tag{C.10}$$

with

$$\begin{aligned} \mathcal{A}_{\pi\pi} &= \chi_\pi \left[\frac{\mathcal{D}_p \mathcal{P}_0 + \mathcal{P}_2}{\mathcal{D}_p} - \frac{\beta}{\alpha c} \left(\frac{1}{\mathcal{P}_3} - \mathcal{H}_\pi \right) \right], \\ \mathcal{A}_{\pi\Delta} &= \chi_{\pi-\Delta} \left[\frac{\mathcal{D}_p \mathcal{P}_0 - \mathcal{P}_1 \sin \Delta + \mathcal{P}_2 \cos \Delta}{\mathcal{D}_p} \right. \\ & \quad \left. - \frac{\beta}{\alpha c} \left[\frac{1}{\mathcal{P}_3} - 1 \right] e^{\frac{\alpha\lambda+1}{\alpha c} \Delta} \right], \\ \mathcal{A}_{\Delta\pi} &= \chi_\pi \left[\frac{\mathcal{D}_p \mathcal{P}_0 + \mathcal{P}_1 \sin \Delta + \mathcal{P}_2 \cos \Delta}{\mathcal{D}_p} \right. \\ & \quad \left. - \frac{\beta}{\alpha c} \left(\frac{1}{\mathcal{P}_3} \right) e^{-\frac{\alpha\lambda+1}{\alpha c} \Delta} \right], \\ \mathcal{A}_{\Delta\Delta} &= \chi_{\pi-\Delta} \left[\frac{\mathcal{D}_p \mathcal{P}_0 + \mathcal{P}_2}{\mathcal{D}_p} - \frac{\beta}{\alpha c} \left(\frac{1}{\mathcal{P}_3} - \mathcal{H}_{\pi-\Delta} \right) \right], \end{aligned}$$

and

$$\begin{aligned} \mathcal{H}_\pi &= \begin{cases} 1, & \text{if } \psi(\pi) > \phi(\pi), \\ 0, & \text{if } \psi(\pi) < \phi(\pi), \end{cases} \\ \mathcal{H}_{\pi-\Delta} &= \begin{cases} 1, & \text{if } \psi(\pi - \Delta) < \phi(\pi - \Delta), \\ 0, & \text{if } \psi(\pi - \Delta) > \phi(\pi - \Delta). \end{cases} \end{aligned}$$

Now in order to examine the stability, we look for nontrivial solutions of $\psi - \phi = \mathcal{A}_p(\psi - \phi)$ such that $\mathcal{E}(\lambda) = 0$, where $\mathcal{E}(\lambda) = \det(\mathcal{A}_p - I)$, is the Evans function of the traveling pulse solution (B.1) and (B.2). The traveling pulse will surely not be linearly stable in the case that $\lambda > 0$ for all real λ such that $\mathcal{E}(\lambda) = 0$. We cannot ensure linear stability, since we have omitted eigensolutions with complex eigenvalues. However, we find that, in many instances, our analysis accurately predicts the nonlinear stability of the associated stimulus-locked traveling pulse. The Evans function is then piecewise defined for four possible classes of eigenfunction: (i) $\psi(\pi) > \phi(\pi)$ and $\psi(\pi - \Delta) > \phi(\pi - \Delta)$; (ii) $\psi(\pi) > \phi(\pi)$ and $\psi(\pi - \Delta) < \phi(\pi - \Delta)$; (iii) $\psi(\pi) < \phi(\pi)$ and $\psi(\pi - \Delta) > \phi(\pi - \Delta)$; and (iv) $\psi(\pi) < \phi(\pi)$ and $\psi(\pi - \Delta) < \phi(\pi - \Delta)$.

References

- Abraham, H. D. (1983). Visual phenomenology of the LSD flashback. *Archives of General Psychiatry*, 40(8), 884–889.
- Abraham, H. D., & Duffy, F. H. (1996). Stable quantitative EEG difference in post-LSD visual disorder by split-half analysis: Evidence for disinhibition. *Psychiatry Research*, 67(3), 173–187.
- Abraham, H. D., & Duffy, F. H. (2001). EEG coherence in post-LSD visual hallucinations. *Psychiatry Research*, 107(3), 151–163.
- Abraham, H. D., & Wolf, E. (1988). Visual function in past users of LSD: Psychophysical findings. *Journal of Abnormal Psychology*, 97(4), 443–447.
- Amari, S. (1977). Dynamics of pattern formation in lateral-inhibition type neural fields. *Biological Cybernetics*, 27(2), 77–87.
- Ben-Yishai, R., Bar-Or, R. L., & Sompolinsky, H. (1995). Theory of orientation tuning in visual cortex. *Proceedings of the National Academy of Sciences of the United States of America*, 92(9), 3844–3848.
- Ben-Yishai, R., Hansel, D., & Sompolinsky, H. (1997). Traveling waves and the processing of weakly tuned inputs in a cortical network module. *Journal of Computational Neuroscience*, 4(1), 57–77.
- Benda, J., & Herz, A. V. M. (2003). A universal model for spike-frequency adaptation. *Neural Computation*, 15(11), 2523–2564.
- Boyer, E. W., & Shannon, M. (2005). The serotonin syndrome. *New England Journal of Medicine*, 352(11), 1112–1120.
- Bressloff, P., Cowan, J., Golubitsky, M., Thomas, P., & Wiener, M. (2001). Geometric visual hallucinations, Euclidean symmetry and the functional architecture of striate cortex. *Proceedings of the Royal Society of London. Series B, Biological Sciences*, 356(1407), 299–330.

- Bressloff, P. C., & Cowan, J. D. (2002). An amplitude equation approach to contextual effects in visual cortex. *Neural Computation*, 14(3), 493–525.
- Bressloff, P. C., & Kilpatrick, Z. P. (2011). Two-dimensional bumps in piecewise smooth neural fields with synaptic depression. *SIAM Journal of Applied Mathematics*, 71(2), 379–408.
- Chervin, R. D., Pierce, P. A., & Connors, B. W. (1988). Periodicity and directionality in the propagation of epileptiform discharges across neocortex. *Journal of Neurophysiology*, 60(5), 1695–1713.
- Chossat, P., & Faugeras, O. (2009). Hyperbolic planforms in relation to visual edges and textures perception. *PLoS Computational Biology*, 5(12), e1000625.
- Cohen, S., & Ditman, K. S. (1963). Prolonged adverse reactions to lysergic acid diethylamide. *Archives of General Psychiatry*, 8(5), 475–480.
- Coombes, S. (2005). Waves, bumps, and patterns in neural field theories. *Biological Cybernetics*, 93(2), 91–108.
- Coombes, S., & Owen, M. R. (2004). Evans functions for integral neural field equations with Heaviside firing rate function. *SIAM Journal on Applied Dynamical Systems*, 3(4), 574–600.
- Coombes, S., & Owen, M. R. (2005). Bumps, breathers, and waves in a neural network with spike frequency adaptation. *Physics Review Letters*, 94(14), 148102.
- Coombes, S., & Schmidt, H. (2010). Neural fields with sigmoidal firing rates: Approximate solutions. *Discrete and Continuous Dynamical Systems A*, 28(4), 1369–1379.
- Dubois, J., & VanRullen, R. (2011). Visual trails: Do the doors of perception open periodically? *PLoS Biology*, 9(5), e1001056.
- Ermentrout, G. B., & Cowan, J. D. (1979). A mathematical theory of visual hallucination patterns. *Biological Cybernetics*, 34(3), 137–50.
- Ermentrout, G. B., Jalićs, J. Z., & Rubin, J. E. (2010). Stimulus-driven traveling solutions in continuum neuronal models with a general smooth firing rate function. *SIAM Journal of Applied Mathematics*, 70(8), 3039–3064.
- Faugeras, O., Veltz, R., & Grimbert, F. (2009). Persistent neural states: Stationary localized activity patterns in the nonlinear continuous n -population, q -dimensional neural networks. *Neural Computation*, 21, 147–187.
- Folias, S. E., & Bressloff, P. C. (2004). Breathing pulses in an excitatory neural network. *SIAM Journal on Applied Dynamical Systems*, 3(3), 378–407.
- Folias, S. E., & Bressloff, P. C. (2005a). Breathers in two-dimensional neural media. *Physics Review Letters*, 95(20), 208107.
- Folias, S. E., & Bressloff, P. C. (2005b). Stimulus-locked traveling waves and breathers in an excitatory neural network. *SIAM Journal of Applied Mathematics*, 65(6), 2067–2092.
- Fontenelle, L. F. (2008). Topiramate-induced palinopsia. *Journal of Neuropsychiatry and Clinical Neurosciences*, 20(2), 249–250.
- Frosch, W. A., Robbins, E. S., & Stern, M. (1965). Untoward reactions to lysergic acid diethylamide (LSD) resulting in hospitalization. *New England Journal of Medicine*, 273, 1235–1239.
- Guo, Y., & Chow, C. C. (2005). Existence and stability of standing pulses in neural networks: I. Existence. *SIAM Journal on Applied Dynamical Systems*, 4(2), 217–248.
- Halpern, J. H., & Pope, H. G. (2003). Hallucinogen persisting perception disorder: What do we know after 50 years? *Drug and Alcohol Dependence*, 69(2), 109–119.
- Hansel, D., & Sompolinsky, H. (1998). Modeling feature selectivity in local cortical circuits. In C. Koch, & I. Segev (Eds.), *Methods in neuronal modeling: From ions to networks* (chap. 13, pp. 499–567). Cambridge: MIT.
- Horowitz, M. L. (1969). Flashbacks: Recurrent intrusive images after the use of LSD. *American Journal of Psychiatry*, 126(4), 565–569.
- Huang, X., Troy, W. C., Yang, Q., Ma, H., Laing, C. R., Schiff, S. J., et al. (2004). Spiral waves in disinhibited mammalian neocortex. *Journal of Neuroscience*, 24(44), 9897–9902.
- Hubel, D. H., & Wiesel, T. N. (1977). Ferrier lecture. Functional architecture of macaque monkey visual cortex. *Proceedings of the Royal Society of London. Series B, Biological Sciences*, 198(1130), 1–59.
- Ihde-Scholl, T., & Jefferson, J. W. (2001). Mitrzapine-associated palinopsia. *Journal of Clinical Psychiatry*, 62(5), 373.
- Kawasaki, A., & Purvin, V. (1996). Persistent palinopsia following ingestion of lysergic acid diethylamide (LSD). *Archives of Ophthalmology*, 114(1), 47–50.
- Kilpatrick, Z. P., & Bressloff, P. C. (2010a). Binocular rivalry in a competitive neural network with synaptic depression. *SIAM Journal on Applied Dynamical Systems*, 9, 1303–1347.
- Kilpatrick, Z. P., & Bressloff, P. C. (2010b). Effects of synaptic depression and adaptation on spatiotemporal dynamics of an excitatory neuronal network. *Physica D*, 239(9), 547–560. Mathematical neuroscience.
- Kilpatrick, Z. P., & Bressloff, P. C. (2010c). Stability of bumps in piecewise smooth neural fields with nonlinear adaptation. *Physica D*, 239(12), 1048–1060.
- Kilpatrick, Z. P., Folias, S. E., & Bressloff, P. C. (2008). Traveling pulses and wave propagation failure in inhomogeneous neural media. *SIAM Journal on Applied Dynamical Systems*, 7(1), 161–185.
- Kishimoto, K., & Amari, S. (1979). Existence and stability of local excitations in homogeneous neural fields. *Journal of Mathematical Biology*, 7, 303–318.
- Kraus, R. P. (1996). Visual “trails” with nefazodone treatment. *American Journal of Psychiatry*, 153(10), 1365–1366.
- Laing, C. R., & Troy, W. C. (2003). PDE methods for nonlocal models. *SIAM Journal on Applied Dynamical Systems*, 2(3), 487–516.
- Lerner, A. G., Finkel, B., Oyffe, I., Merenzon, I., & Sigal, M. (1998). Clonidine treatment for hallucinogen persisting perception disorder. *American Journal of Psychiatry*, 155(10), 1460.
- Lerner, A. G., Skladman, I., Kodesh, A., Sigal, M., & Shufman, E. (2001). LSD-induced hallucinogen persisting perception disorder treated with clonazepam: Two case reports. *Israel Journal of Psychiatry and Related Sciences*, 38(2), 133–136.
- Madison, D. V., & Nicoll, R. A. (1984). Control of the repetitive discharge of rat CA1 pyramidal neurones *in vitro*. *Journal of Physiology*, 354, 319–331.
- Moskowitz, D. (1971). Use of haloperidol to reduce lsd flashbacks. *Military Medicine*, 136(9), 754–756.
- Nichols, C. D., & Sanders-Bush, E. (2002). A single dose of lysergic acid diethylamide influences gene expression patterns within the mammalian brain. *Neuropsychopharmacology*, 26(5), 634–642.
- Oster, G. (1970) Phosphenes. *Scientific American*, 222(2), 82–87.
- Pinto, D. J., & Ermentrout, G. B. (2001). Spatially structured activity in synaptically coupled neuronal networks: I. Traveling fronts and pulses. *SIAM Journal on Applied Mathematics*, 62(1), 206–225.
- Rosenthal, S. H. (1964). Persistent hallucinosis following repeated administration of hallucinogenic drugs. *American Journal of Psychiatry*, 121, 238–244.

- Shusterman, V., & Troy, W. C. (2008). From baseline to epileptiform activity: A path to synchronized rhythmicity in large-scale neural networks. *Physical Review E*, 77(6), 061911.
- Stocker, M., Krause, M., & Pedarzani, P. (1999). An apamin-sensitive Ca^{2+} -activated K^{+} current in hippocampal pyramidal neurons. *Proceedings of the National Academy of Sciences of the United States of America*, 96(8), 4662–4667.
- Troy, W. C., & Shusterman, V. (2007). Patterns and features of families of traveling waves in large-scale neuronal networks. *SIAM Journal on Applied Dynamical Systems*, 6(1), 263–292.
- Tsai, P. H., & Mendez, M. F. (2009). Akinetopsia in the posterior cortical variant of Alzheimer disease. *Neurology*, 73(9), 731–732.
- Wilson, H. R., & Cowan, J. D. (1972). Excitatory and inhibitory interactions in localized populations of model neurons. *Biophysics Journal*, 12(1), 1–24.
- York, L. C., & van Rossum, M. C. W. (2009). Recurrent networks with short term synaptic depression. *Journal of Computational Neuroscience*, 27(3), 607–620.
- Young, C. R. (1997). Sertraline treatment of hallucinogen persisting perception disorder. *Journal of Clinical Psychiatry*, 58(2), 85.
- Zhang, L. (2004). Existence, uniqueness and exponential stability of traveling wave solutions of some integral differential equations arising from neuronal networks. *Journal of Differential Equations*, 197(1), 162–196.